Chapter 1

Background & Introduction

1.1 History of Perovskite

A plethora of research work is carrying out using perovskites. Its easy synthesis, stability in harsh conditions and easily modifiable crystal structure with a series of perovskite family keeps it in demand. Thus, it is imperative to understand the basics of perovskites and then build on that knowledge to obtain desired results. Perovskites lie in the crystalline structures of the ternary family, having a general formula ABX_3. X anions are preferentially oxygen anions that are densely packed at two kinds of sites. One is forming octahedra, i.e., coordinated with six cations, while the other is coordinating with eight or twelve cations. Smaller cations with variable oxidation states can be lodged in the octahedral sites (mostly transition metals), and comparatively large-sized mono-, di- or tri-valent cations can occupy the eight or twelve coordinated sites (preferably alkaline earth metals). Latter cation is denoted by A cations, which has cuboctahedral coordination having twelve X anions at its 12 vertices. The former cation is represented as B cations present in octahedral coordination(Moure and Peña 2015). Peculiarly, two B-site cations and four A-site cations surround each X anion shown in figure 1.1. This crystal structure provides a lot of tailoring opportunities, resulting in compounds having a wide range of chemical formulas, properties, and applications, as summarized in Table 1.1.

The mineral perovskite ($CaTiO_3$) was discovered in the Ural Mountains, Russia in 1839 by Gustav Rose, the German chemist and mineralogist. However, it was named perovskites in honor of the Russian mineralogist and military officer Lev Alexeievitch Perovsky (Structure-Property Relations in Rare-Earth Doped Manganite Perovskites 2019).

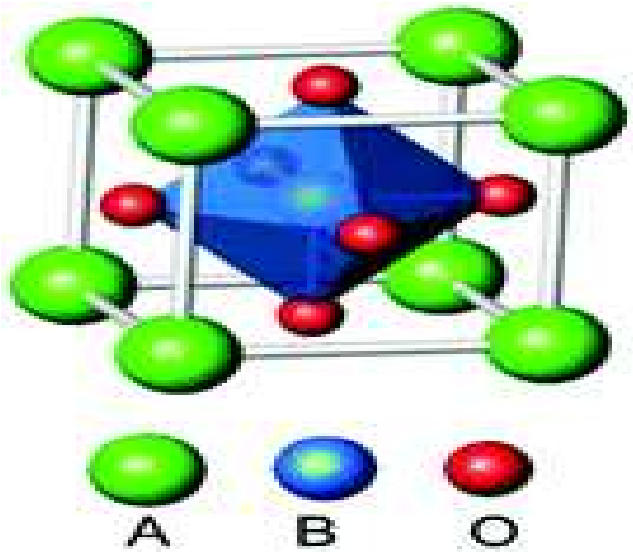

Figure 1.1 shows the Perovskite structure (Rabuffetti and Brutchey 2014)

1.2 High dielectric constant ABO_3 Perovskite

(a) Calcium Titanate $CaTiO_3$

It is observed that at room temperature $CaTiO_3$ behaves as paraelectric material. However, when it is doped with cation, its dielectric constant increases as the result of an increase in the boundary layer effects. Ceramics are very sensitive to dopants and the sintering process. The temperature is a crucial factor in determining the geometry of $CaTiO_3$. At room temperature, it exists as orthorhombic and changes to tetragonal at 600˚C and cubic at 1000˚C. Through the studies of the conductivities in the oxidizing atmosphere at the temperature of 130℃, it is established that it shows p-type semiconductor behavior (Ali and Yashima 2005).

(b) Barium Titanate ($BaTiO_3$)

It is recognized that the high dielectric constant of $BaTiO_3$ is the consequence of its ferroelectric behavior. The face-centered cubic arrangement of atoms observed in

$BaTiO_3$ is due to the same ionic radii of barium and oxygen (1.4 Å). While Ti occupies the B sites of the perovskite surrounded by six oxide ions forming an octahedron. Tetrahedron shifts either up or down, creating a non-centrosymmetric structure responsible for ferroelectricity. Additionally, electronic polarization is also generated in the structure due to the high oxidation state and low energy vacant d-orbitals of Titanium. Moreover, three phase transitions were observed on cooling and during the transition, a shift of 0.1 Å is noticed. Orientation of spontaneous polarization rearranges with these phase transitions. At room temperature, it exists as a tetragonal structure, at temperature reaches upto 1450°C it exists as hexagonal structure and below it is present in cubic structure having paraelectric character. At curie temperature, $BaTiO_3$ displays temperature-dependent dielectric constant (Smith et al. 2008; Bassat et al. 2013; A. Molina-García and V. Rees 2016).

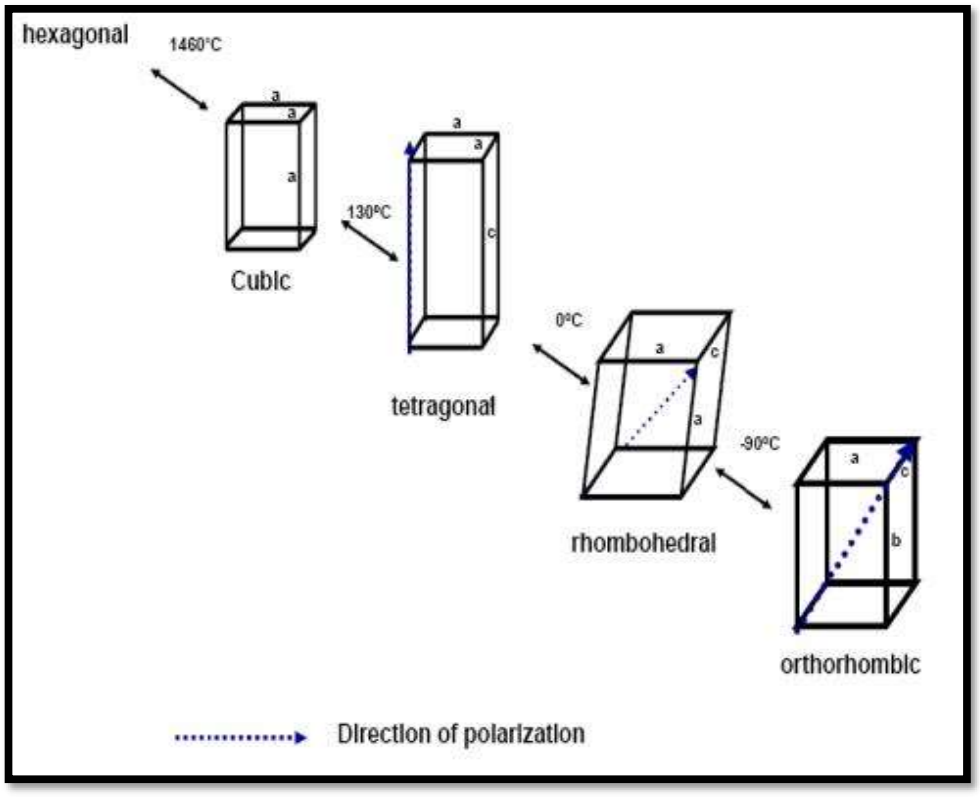

Figure 1.2 Phase diagram for conversion of $BaTiO_3$ Perovskite structure

(c) Strontium Titanate $SrTiO_3$

This ceramic is widely used as high-temperature superconductor thin film, in water photolysis, Oxygen sensor and magneto hydrodynamic operators, memory devices, optical processes. (Zhuk et al. 2018) The n-type semiconducting behavior is the result of oxygen. At room temperature, $SrTiO_3$ exists in a cubic structure with a band gap of 3.2 eV and consists of paraelectric properties. Doping SrTiO3 with rare earth metals increases dielectric constant with relaxor behavior (Banerjee et al. 2006. For example, the dielectric constant of SrTiO3 is 300, which rises to 18000 on doping with Yttrium (Amow et al. 2006; Carrasco et al. 2006; Allison 2007; Sharma et al. 2014).

Over the last decade, extensive experimental and theoretical work on perovskite-based materials has demonstrated a strong interrelationship between distortions of the crystal structure and many processes and phenomena such as photoluminescence, ferroelectric, piezoelectric, and pyroelectric properties.

As per Goldschmidt, the stability of the structure of perovskite-type phase for a particular group of cations and anions is determined by the tolerance (t) factor. This parameter signifies the symmetry of the crystal system and appreciably determines its dielectric properties. The t-factor is a variable concerning the limits for the size of cations and permits the perovskite-type phase formation.

The tolerance (t) factor is given by following equation(Tidrow 2014):

$$t = \frac{r_A + r_0}{\sqrt{2}(r_B + r_0)} \tag{1.1}$$

Where r_A, r_B and r_O respectively represent the radii of A, B (cation), and O (anion). The relation between tolerance (t) factor and geometry is provided in following table 1.2.

Table 1.1 Properties of perovskites and their applications

Property	Application	Materials
Proton conductivity	SOFC electrolyte	$BaZrO_3$, $SrCeO_3$
Ionic conductivity	Solid electrolyte Hydrogen sensor H2 production/extraction	$(La,Sr)(Ga,Mg)O_{3-d}$
Mixed conductivity	SOFC electrode Piezoelectric transducer	$La(Sr,Ca)MnO_{3-d}$, $LaCoO_3$ $(La,Sr)(Co,Fe)\ O_{3-\delta,}$ $BaTiO_3$,
Ferroelectric/piezoelectric	Thermistor, actuator Thin film resistor	$GdFeO_3$, $LaMnO_3$
Magnetic	Magnetic memory Ferromagnetism	$GdFeO_3$, $LaMnO_3$
Electrical/dielectric	Multilayer capacitor Dielectric resonator Thin film resistor	$BaTiO_3$, $BaZrO_3$
Superconductivity	Superconductor	$Ba(Pb,Bi)O_3$ $YBa_2Cu_3O_{7-\delta}$
Optical	Electrooptical modulator Laser	$(Pb,La)(Zr,Ti)O_3$, $YAlO_3$, $KNbO_3$
Catalytic	Catalyst	$LaFeO_3$, $La(Ce,Co)O_3$

Table 1.2 Structure of perovskite oxide based on Tolerance factor (Yadava et al. 2017)

Tolerance factor	Structure of perovskite oxide
≥1	Ferroelectric and hexagonal
0.95≤ t ≤1.0.	Cubic
0.75<t<0.95	Non-ferroelectric with distorted structure.
t<0.75	Not a perovskite

1.3 Perovskite Structure and Derivatives

1.3.1 Cubic Perovskites

As already mentioned, the general formula representing a perovskite is ABO_3, where O is oxide ion and cations are denoted by A and B alphabets. The symmetric structure of a perovskite can be easily visualized in terms of the BO_6 octahedra sharing corners along all 3 dimensions infinitely. The holes created by 8 BO_6 octahedra are occupied by A cations, forming 12-fold coordination of oxygen around the A cation, and since the B-cation forms BO_6 octahedra, oxygen anions forms 6-fold coordination around it. $SrTiO_3$ shown in figure 1.3 is an example of simple ABO_3 perovskite structure, where the Sr atoms is the 12 coordinated A site, while the Ti atoms represent 6 coordinated B site. it is observed that the ideal cubic structure of many simple ABO_3 perovskites is distorted to acquire lower symmetry(Zhong and Vanderbilt 1995). (e.g., tetragonal, orthorhombic, etc.)

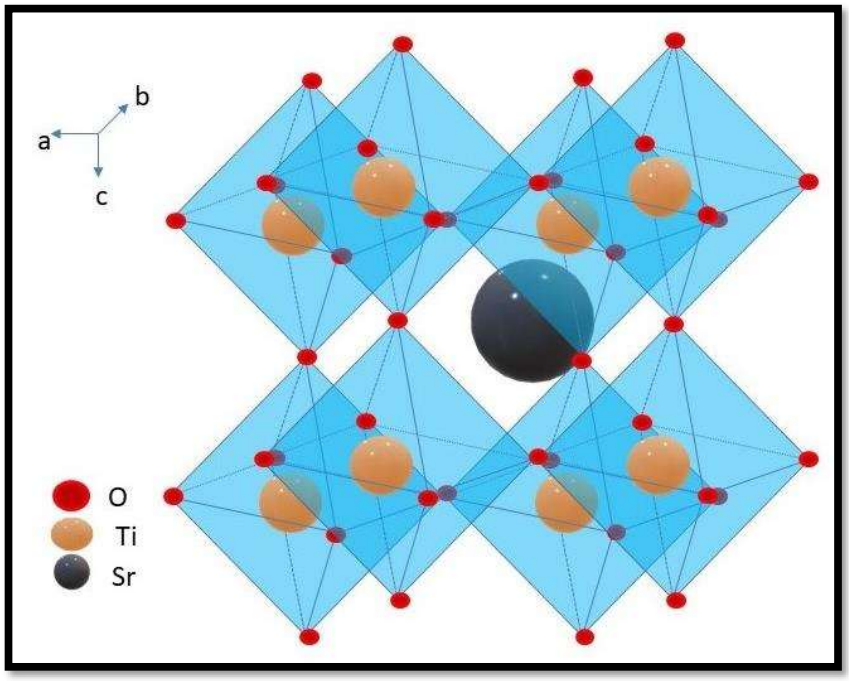

Figure 1.3 shows the cubic Perovskite structure of $SrTiO_3$

1.3.2 Complex perovskite

The simple ABO_3 perovskites have been modified to complex perovskite oxide represented by the general formula $(A'A'')(B'B'')O_3$ through doping. The indefinite possibility of configuration and structure of complex perovskite oxides is possible through vast possibilities of doping with homo or heteroatom which further opens up the chance for a variety of technological applications(Heiland 1954; Ezhilvalavan and Tseng 2000; Hardy et al. 2004; Hao et al. 2009; Dubey et al. 2011). In this type of perovskite oxide, A site of cations is occupied by two different cations represented as A' and A″ which exist as divalent species. However, it can exist as trivalent species in the case of lanthanide or transition metal ions, like La^{+3}, Ce^{+3}, Fe^{+3}, Al^{+3}, Ti^{+3}. Similar to the A site in complex perovskite the B site is also occupied by more than one type of anions existing in tetravalent state like Ti^{+4}, Fe^{+4}, Mn^{+4}, W^{+4}, Nb^{+4}. Alteration possibility in both ions provides a great deal of control over various properties. The complex perovskite sought much attention in the recent decade due to its attractive

results in the area of dielectric and magnetic properties (Lee et al. 2000; Lettieri et al. 2000; Kuo et al. 2001). Other additional perovskite known to exist as homologous series of $A_{n+1}B_nO_{3n+1}$, $A_nB_nO_{3n+1}$(Dion et al. 1981; Holtzworth-Munroe and Jacobson 1985), $Bi_2A_{n-1}B_nO_{3n+3}$ (Aurivillius series) (B. Aurivillius 1949; B. Aurivillius 1950; B. Aurivillius 1951). Few anions deficient perovskites represented by formula $A_nB_nO_{3n-2}$ related to ABO_3 perovskite are also reported. Ruddlesden-Popper and Dion-Jacobson explained a variety of technological applications of these perovskite oxides, such as multiferroic, magneto-resistant materials, ferroelectrics, ionic conductors, superconductors, the amount of defect, and their mutual interaction.

1.3.2 (a) Double Perovskites

The double perovskite structure got its name due to the presence of twice the unit cell ($A_2B_2O_6$) that of perovskite (ABO_3). Here also, A site 12 coordinated and B sites 6 coordinated having the same architecture, but 2 cations occupy the B site. The structure of Sr_2FeMoO_6 is shown in figure 1.4. The arrangement of Fe and Mo atoms in a 3D space is ordered in a chessboard type pattern(García-Landa et al. 1999).

(b) Layered Perovskties: Ruddleson-Popper, Aurivillius and Dion-Jacobson phases

The characteristics feature in the structure of Layered perovskites is the presence of infinite 2D slabs of the simplest ABO_3 perovskite type structure separated by specific motif and layers having the general formula: $A_{(n-1)}B_{(n)}O_{(3n+1)}$. The layered perovskites are distinguished on the basis of the following characteristics(Lemmerer and Billing 2010):

1) The specific motif that separates the layers,

2)The layers offsetting from one another.

In the formula given above, "n" denotes the length of the two-dimensional (2D) slabs. n=1 indicates the slab has thickness of only one BO_6 octahedron. n=2 indicates the thickness of two BO_6 octahedra, so on.

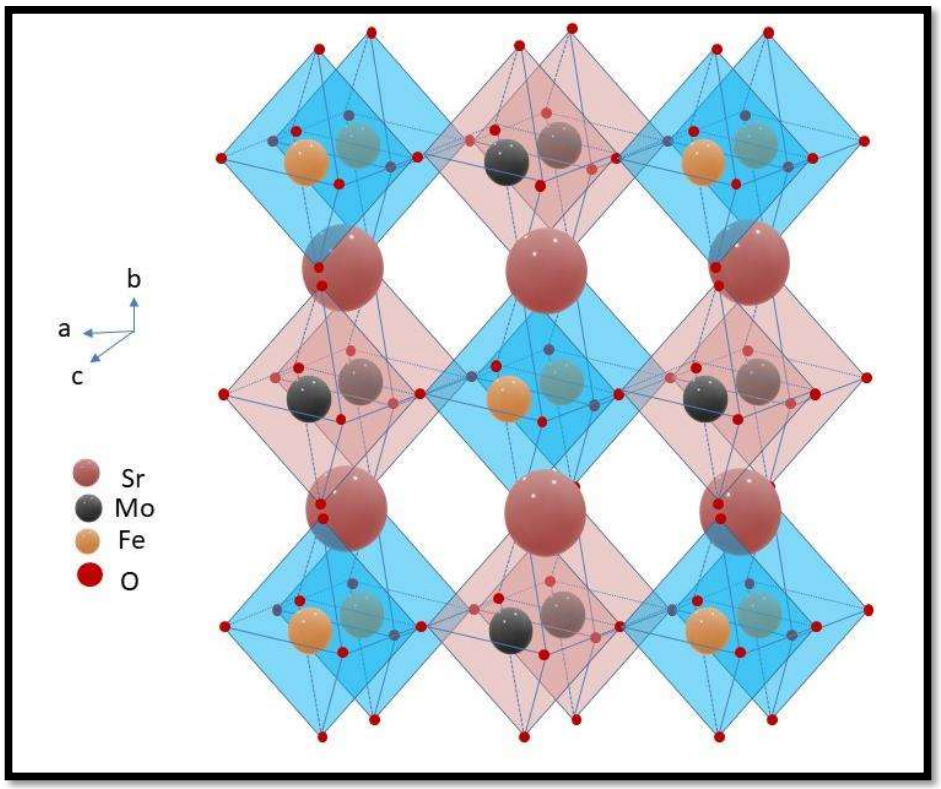

Figure 1.4 shows the double perovskite structure of Sr_2FeMoO_6.

The clear examples are the n=1 in Sr_2RuO_4 and n=2 in $Sr_3Ru_2O_7$ Ruddleson-Popper phases, as shown in figure 1.5. In these phases, the A cation and the B cation are occupied by Sr and Ru cations, respectively. The Sr_2 layer acts as the separating motif, and the perovskite slabs layers are offset by a translation of (1/2,1/2). The Ruddleson Popper phases have the general formula $(A_{(n+1)}B_nO_{(3n+1)})$, indicating the separating A_2 cations as a part of the 2-D perovskite slabs or as $\{A_2\}$-$\{A_{(n-1)}B_nO_{(3n+1)}\}$ as it relates them more appropriately to the other forms of layered perovskites(Iliev et al. 2005).

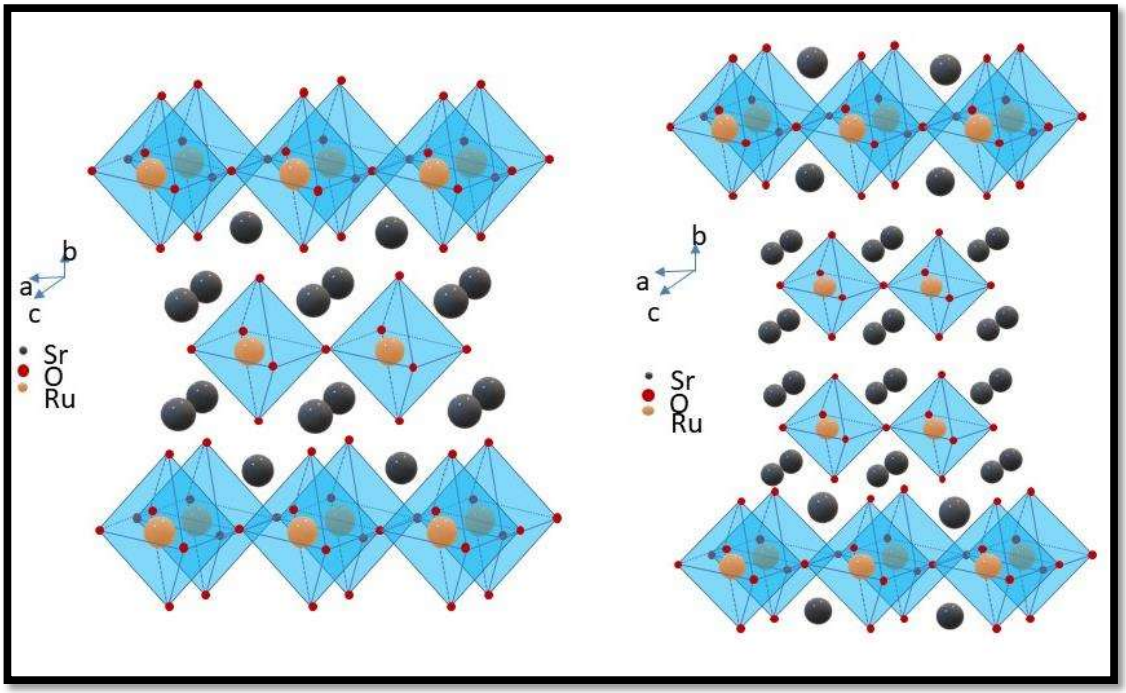

Figure 1.5 shows the n=1 in Sr_2RuO_4 and n=2 in $Sr_3Ru_2O_7$ Ruddleson-Popper phases structure.

The Aurivillius phase is another such layered perovskites having the general formula $\{Bi_2O_2\}$-$\{A_{(n-1)}B_2O_7\}$. The typical example to understand Aurivillius phases, where n=2 is Bi_3TiNbO_9 shown in figure1.6. Here, in this phase on the B sites, Nb and Ti are dispersed statistically. The formula now expressed as: $\{Bi_2O_2\}$-$Bi(Ti,Nb)_2O_7$. In all of the Aurivillius phases, rock-salt Bi_2O_2 layer acts as the separating motif. For this example, the A site in the layer is also occupied by Bi cations, which needn't be the case in all the Aurivillius phases. The displacement in these phases among the perovskite slabs is (1/2,1/2) translation(Xu et al. 2016).

The Dion-Jacobson is another form of layered perovskites phases having the general formula as $(M^{+1}A_{(n-1)}B_nO_{(3n+1)})$. The differentiating characteristics of these phases from the other forms of layered phases are the presence of alkali metal acting as the separating motif between the layers. The common example of Dion-Jacobson phase is

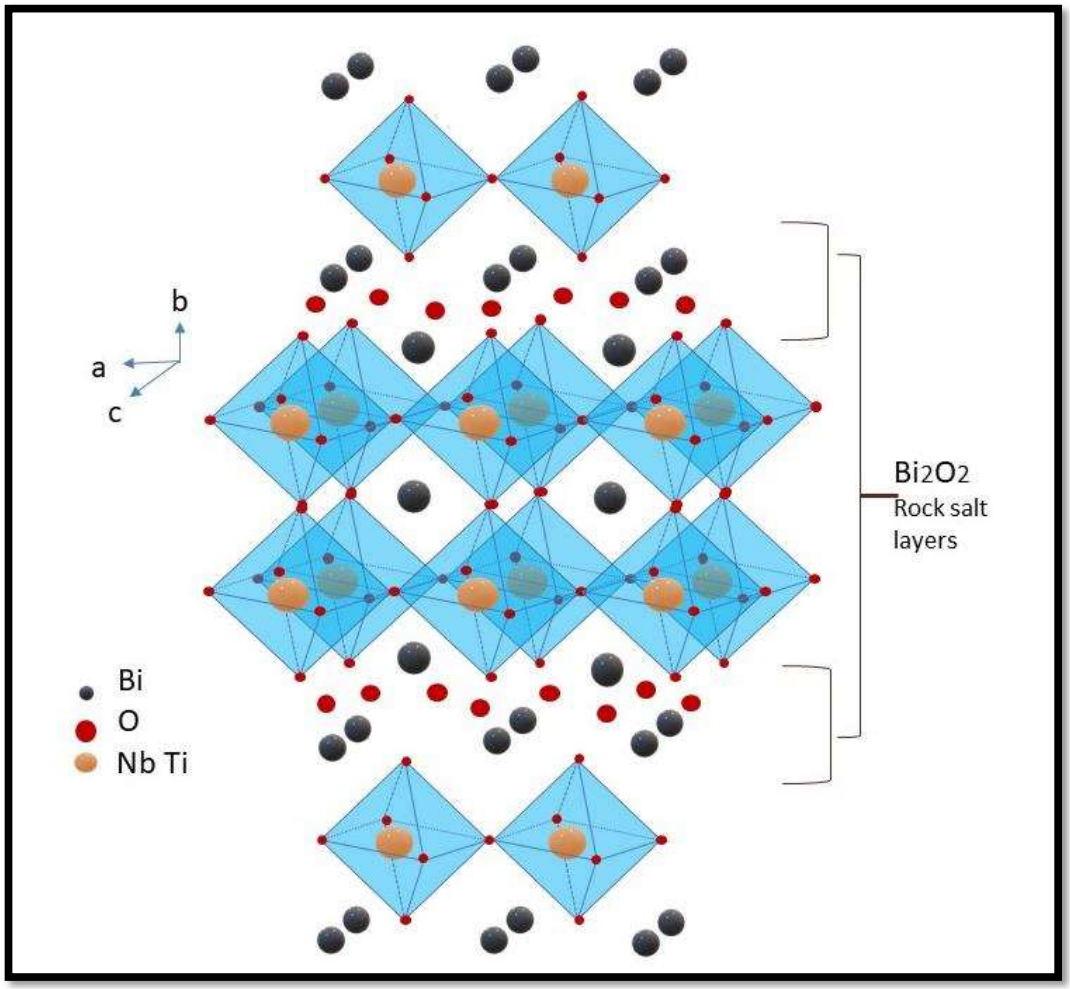

Figure 1.6 shows Aurivillius phases structure of is Bi_3TiNbO_9, where n=2.

$CsLaNb_2O_7$ shown in figure 1.7. The specific alkali metal in the phase decides the displacement among the perovskite slabs, which can be either (1/2,0) or no displacement at all (Yoo et al. 2018).

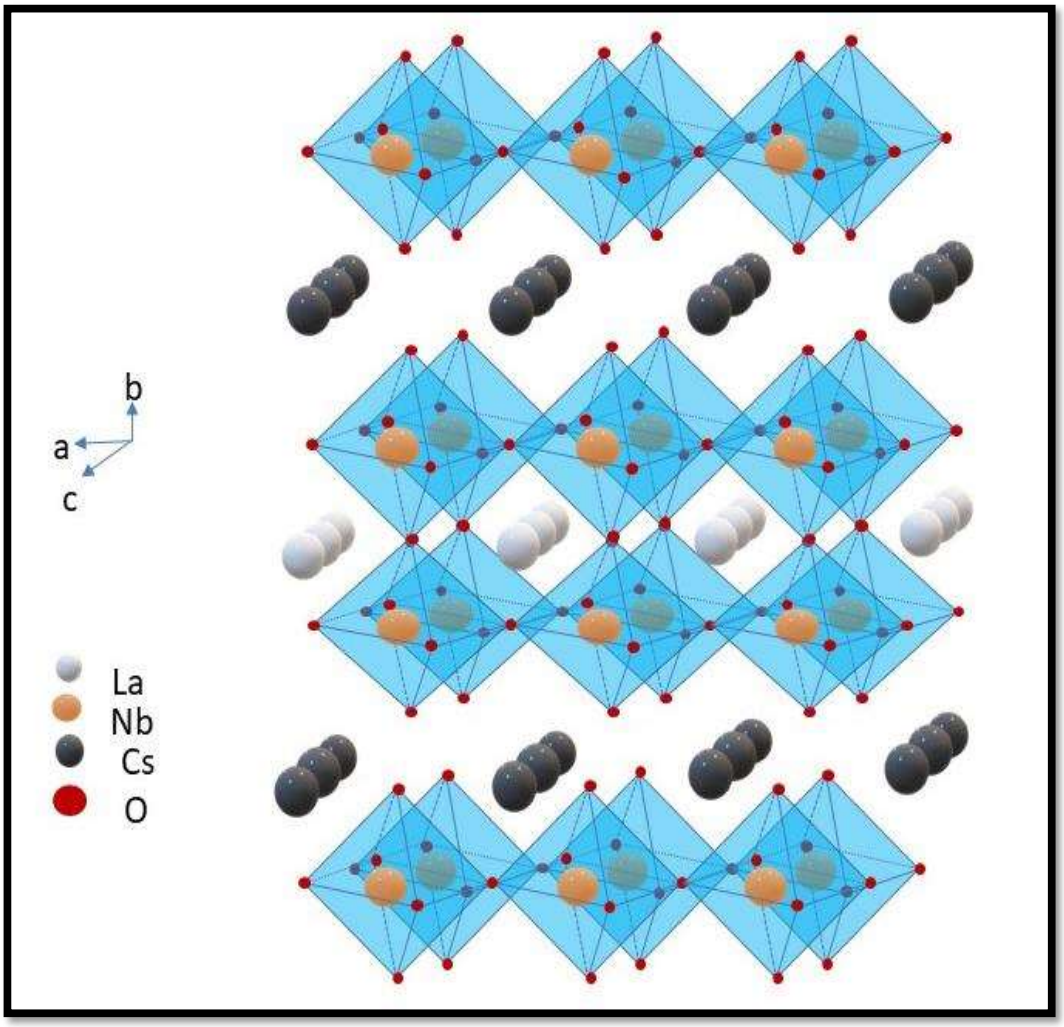

Figure 1.7 shows of $CsLaNb_2O_7$ Dion-Jacobson phase structure.

1.4 Applications of Pervoskites Oxides:

Since the perovskite structure can accommodate a variety of cations and anions that change its structure and properties, deep interest in this class of materials has emerged. These compounds form a large group of dielectric materials having ferroelectric, antiferroelectric, and paraelectric behavior at room temperature. Members of the perovskite family of type I ($A^{1+}B^{5+}O_3$) find applications in electro-optic devices due to their large electro-optic coefficients at room temperature. Due to large acoustic coefficients at room temperature, $KNbO_3$ and $KTaO_3$ of the above family are used in acousto-optic devices $LiNbO_3$, $LiTaO_3$, and $KTaO_3$ are used as electro-optic materials,

microwave surface acoustic devices, and holography memory devices. Compounds of family $A^{2+}B^{4+}O_3$ exhibit piezoelectric as well as ferroelectric properties at room temperature. They are used as piezoelectric transducers, phonographs, air transducers, instrument transducers, underwater sound, and ultrasonic power wave filters, delay line transducers, gas lighter elements, dynamic and blast gauges accelerometers, and high voltage sources. They are also used for sound transmission and reception, ultrasonic cleaning devices, information storage in electronic computers, and dielectric amplifiers. (Chandler et al. 1993) Another important perovskite oxide of this family is $SrTiO_3$ which can be used as grain boundary barrier layer capacitors (GBBLC) and positive temperature coefficient (PTC) thermistors. It also finds application in the photolysis of water, gas sensor and magneto hydrodynamic (MHD) applications. Thin films of $BaSnO_3$ deposited on Al_2O_3 substrate are used for 21 sensing CO_2 and nitrogen dioxide gases at constant partial pressure. $SrSnO_3$ is used as a humidity sensing material. $BaSnO_3$ and its solid solutions with titanates have also found applications in the fabrication of ceramic boundary layer capacitors. Barium-based B-site substituted compounds are used as microwave resonators in cellophane. Pb-based B-site substituted compounds are used as multilayer capacitors for miniaturization and in the electronic industry.

Table 1.3 An example of some perovskite explains property application and its use.

Compounds	**Typical property**	**Application**
$BaTiO_3$, $PdTiO_3$	Ferromagnetic property Piezoelectricity and high dielectric constant.	Multilayer ceramic capacitors (MLCCs), PTCR resistors, and embedded capacitance. Most widely used dielectric ceramic T_C = 125°C
$(Ba,Sr)TiO_3$, $(Bi,Na)TiO_3$	Non-Linear dielectric properties.	Tunable microwave devices. Used in the para-electric state.
$Pb(Zr,Ti)O_3$	Ferromagnetic property Piezoelectricity.	Piezoelectric transducers actuators and ferroelectric memories. PZT most successful piezoelectric material.
$Bi_4Ti_3O_{12}$	Ferroelectric with high Curie temperature.	High-temperature actuators and Ferroelectric Properties. Aurivillius compound T_C = 675°C
$(K_{0.5}Na_{0.5})NbO_3$ $Na_{0.5}Bi_{0.5}TiO_3$	Ferromagnetic property Piezoelectricity.	Lead-free piezo- ceramics. Performances are not yet comparable to PZT but rapid progress.
$SrFeO_3$, $LaCoO_3$	Electrical conductivity.	Alternative dielectric materials and Internal barrier layer capacitors. Multifunctional material
$BiFeO_3$, $LaMnO_3$	Magnetic property.	Magnetic field detectors, Memories. Most investigated multiferroic compound. T_C = 850°C
$LaCoO_3$, $BaCuO_3$	Catalytic property.	Cathode material in SOFCs and oxygen separation membranes. Used for Solid Oxide Fuel Cells cathodes.
$LaAlO_3$, $YAlO_3$	Host materials for rare-earth luminescent ions.	Lasers Substrates for epitaxial film deposition.

1.5 Ceramic Materials

Ceramic materials have been used since ages and have been a crucial part of our everyday lives. Apart from being famous for their inert and thermal stability behavior, They exhibit a variety of other properties too, such as opaque or transparent, and conductor, semiconductor or insulator, rigid or flexible, single crystal or polycrystalline, or composites, high melting or low melting, etc.(Jang et al. 2002). These materials can be inorganic or non-metallic materials. The age-old method of its synthesis is making bricks in chimneys to new world synthesis methods such as solid-state route sol-gel method, hydrothermal method, and semi-wet route (Jacobson et al. 2002 May 1). The most desirable property of ceramic materials is their incomparable insulating properties. Some ceramic materials are known not to conduct electricity but instead get polarized internally and, thus, used to store-in electrical energy in capacitors (Richerson and Lee 1992).

A few examples of ceramics with other properties are Zinc oxide in varistors is an example of electro ceramics, lead zirconium titanate (PZT) applied for piezo-electrics, barium titanate used as capacitors and tin oxide or lead lanthanum zirconium titanate (PLZT), as gas sensors, used in electro-optic devices (Kuczenski and Segal 1989; Cabuk et al. 2007; Cain and Stewart 2014).

1.6 Composite Materials

Composite materials or the compositions of materials are the mixtures of more than one material of different compositions that may be binders, fillers, reinforcement, or may have equally important components functionally. The chemical and physical properties of composite materials are generally different from the individual property of the materials used. Composite materials are widely used in industries for their excellent

resistance to varied forms of corrosion and chemicals. It has also been applied because of various unique properties such as relatively lower mass, lower weight, technological opportunities, and unrivaled manufacturing (Satyanarayana et al. 1990; Pathania et al. 2009). Other desirable properties of the composite materials are their use in electrical applications such as chemical properties, circuit boards, switches, connectors, terminals, etc. Composite materials exhibit excellent electrical as well as mechanical properties, for example, these composite materials are also demanded in parts of the automobile and aerospace industries.

Table 1.4 Physical properties and applications of some ceramic materials.

Material	**Properties**	**Application**
PZT	Change of polarization with change in temperature.	Pyroelectrics
PLZT	Change of birefringence with field	Electro-optics
$BaTiO_3$	high breakdown voltage Change of resistance with temperature, high permittivity	Thermistors Capacitors
Ferrites	Permeability, coercive field	Magnets
ZrO_2	Ionic conductivity	Gas sensors
$LiNbO_3$	High piezoelectric coefficients	Transducers, Piezoelectric.
Al_2O_3, AIN, BeO_3	Low permittivity, High thermal Conductivity,	Substrates, Packaging,

1.7 Capacitors

A capacitor is an electrical component that stores energy on the application of voltage as an electrical charge. It releases the stored energy in the circuit when required. It consists of two metallic parallel plates in which dielectric material is embedded. This dielectric material can be the number of insulating materials or their combinations. The most

commonly used ones are ceramic, glass, Mylar, oil, polypropylene, and polyester. The capacitance of the capacitor embedded with a dielectric material is increased by the factor "k" when compared to air and this factor is called the Dielectric Constant. Thus, a dielectric material is as good insulator as higher is its dielectric constant value.

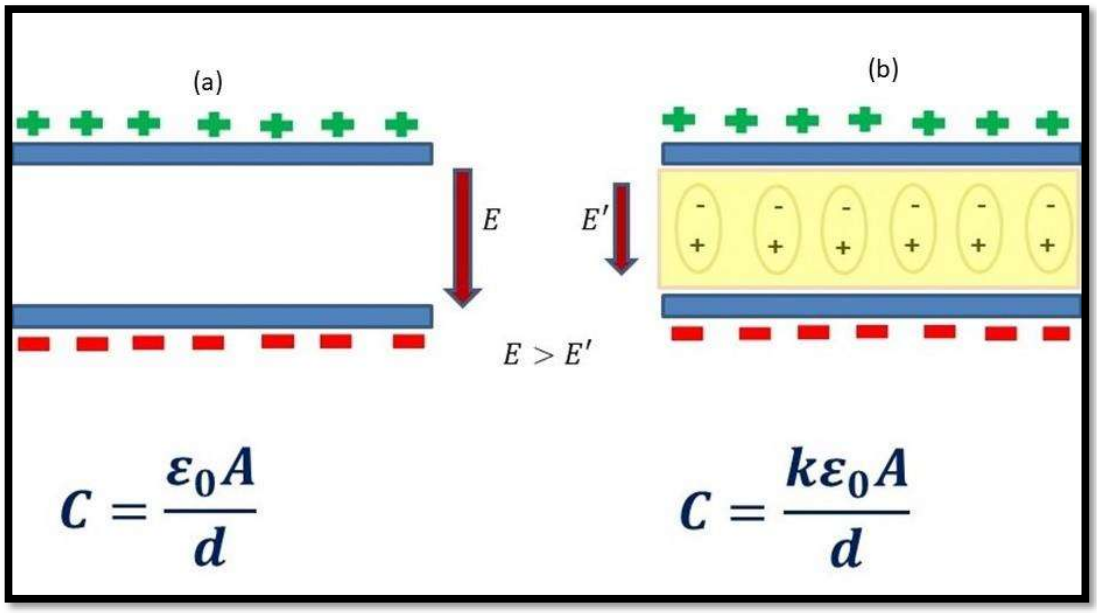

Figure 1.8 Parallel plate capacitor with the plates separated by distance (d) and area of each plate (A).

The dielectric constant is a dimensionless quantity and the actual permittivity of dielectric materials (ε) is the product of the k factor or more correctly relative permittivity(ε_r) and the permittivity of the free space(ε_0) in between the plate. The actual permittivity (ε) of a dielectric material is as follows:

$$\varepsilon = \varepsilon_0 \times \varepsilon_r \tag{1.2}$$

The permittivity of the free space of a vacuum, ε_o, also termed as the "permittivity of a vacuum" has a constant value of 8.84 x 10^{-12} Farads per meter. The relative permittivity value is greater than 1 (ε_r >1), therefore, it can be stated that the capacity of storing charge by a capacitor embedded with a dielectric material is greater than vacuum or the free space under applied external electric fields. Thus, it is always preferable to

substitute the vacuum of free space with some insulating or dielectric material. The capacitance (C) of capacitor embedded with dielectric materials in farads is given by the equation

$$C = \frac{\varepsilon_0 \varepsilon_r A}{d} \tag{1.3}$$

Since it has been established that if the value of the dielectric constant is higher, the capacitance will also be higher. Thus, in practical designing for the miniaturization of the devices, materials of the high dielectric constant are demanded.

1.8 Dielectric materials

Dielectric materials or dielectrics are principally electrically insulating materials or show high resistance to the flow of charge such that when an electric field is applied, no current is allowed to flow through the materials due to the absence of free electrons. However, due to the presence of an electric field equilibrium position of the electric charge or the dipole moment is slightly shifted and aligned in the direction of the electric field resulting in electric polarization in the dielectrics creating an internal electric field. It should be understood that electrical energy that is transferred is due to the shifting of current, not due to conduction. With the use of dielectrics, one can alter the electrical phenomena, i.e., the electrostatic force between two opposite electric charges is significantly minimized and the magnitude of energy stored per unit volume in an electric field is much greater. A capacitor filled with the dielectrics would be much higher than it would be in a vacuum.

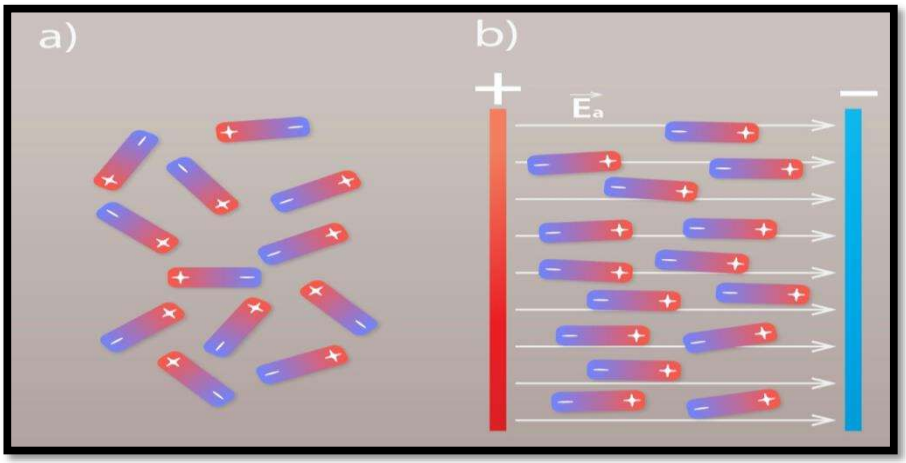

Figure 1.9 (a)non- polarized plates and (b) polarized and of an applied electric field.

1.9 Types of Polarization

There are four primary mechanisms of polarization:

1.9.1 Electronic or Atomic Polarization: Atomic Polarization is shown by all sort of dielectric materials. On application of external electric field(E) charge on each atom in the material gets separated and consequently, the center of the electron cloud around the nucleus in an atom gets slightly shifted and polarization of atoms occurs with dipole moment (P). the magnitude of polarization, as expressed in equation 1.3 is dependent on the magnitude of the applied electric field and a factor called polarizability(α), which property of the atoms

$$P = \alpha E \tag{1.4}$$

As soon as the electric field is eliminated, electron clouds and nuclei resume their original position. The total magnitude of polarization is smaller when compared to other forms of polarization mechanism due to slight displacement in charges (Koops 1951; Bai et al. 2000: 200; Cohen et al. 2003; Kretly et al. 2003; Balamurugaraj et al. 2013; D.W. Richerson et al 1992; Boukenter et al 1988).

1.9.2 Ionic Polarization: This polarization type is generally shown by ionic solids and it makes a significant contribution to relative permittivity. Net polarization is not shown

by the material when no external field is applied as the dipole moment of the counter ions cancel each other due to the presence of symmetry in the crystals. On the other hand, in the presence of an external electric field, polarization is induced in the materials because the ions displace from their equilibrium positions. As a result, the net dipole moment is exhibited by the material.

1.9.3 Dipolar or Orientation Polarization: The type of materials having permanent dipole moment in the same direction as the applied electric field generates Orientation Polarization. An example of such material being HCl and H_2O etc and charge distribution within these molecules creates a permanent dipole moment (Rosenberg et al 1988). In the case of H_2O, hydrogen atoms are slightly positively charged and oxygen atoms are negatively charged, making water molecules dipolar. When the material is present in the absence of an electric field, no net dipole moment is shown due to the cancellation of dipole moment as a result of thermal agitation within the molecules. However, when an external electric field is operated, the molecules begin to reorient in the direction of the external field, generating a net dipole moment in the material.

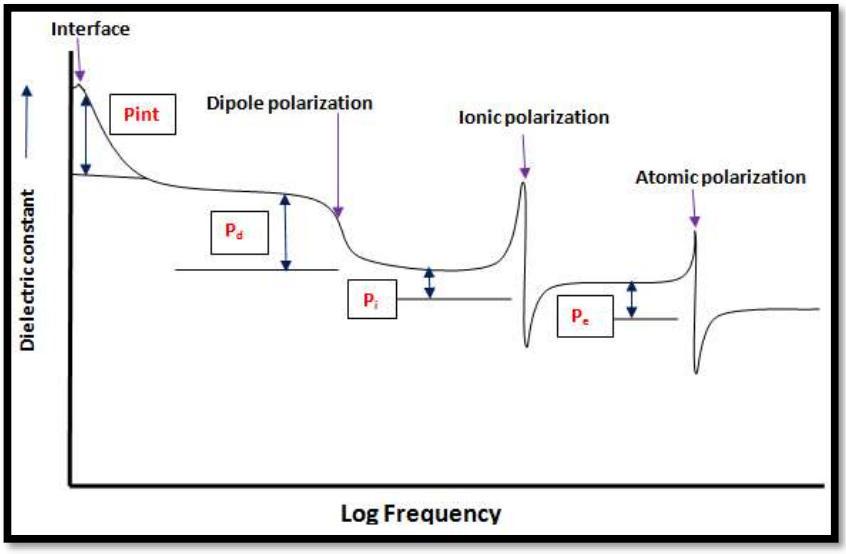

Figure 1.10 Schematic figures between dielectric constant vs log (frequency) showing various mechanisms.

Table 1.5 Polarization mechanism of dielectric materials

Polarization Mechanism					
Type of polarization	**No E field (E=0)**	**Local E Field (E≠0)**	**Case where it is Observed**	**Frequency range where it is predominant**	**Strength of Polarization**
Interfacial Polarization	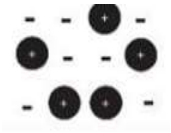	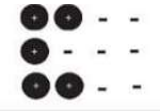	Heterogeneous Systems	10^{-3} to 10^{3} Hz	Very strong
Molecular or Orientation or Dipolar Polarization	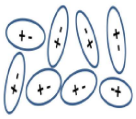	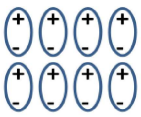	Molecules with permanent dipole moment	10^{11} to 10^{12} Hz	Weak
Ionic polarization		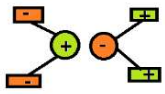	Ionic species	10^{12} to 10^{13} Hz	Strong
Electronic Polarization	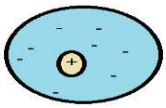	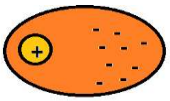	Neutral atoms	~ 10^{15} Hz	Very weak

1.9.4 Interface or Space Charge Polarization: When the material gets polarized under the influence of an external electric field due to the movement of charges is referred to as Interface or Space Charge Polarization. This type of polarization generally results from the charge accumulation at the interface of two different materials or grain boundaries within the material and is usually shown by polycrystalline or amorphous solids. The reasons for the formation of space charges could be charges randomly generated by cosmic radiation or charges that get entrapped in the material during the synthesis process or created by thermal deterioration (D.W. Richerson et al 1992).

The scheme depicted in figure 1.10 helps to interpret which polarization is significant in the material concerned from the experimental data.

1.10 Dielectric Constant

As discussed above relative permittivity or specific inductive capacity is more commonly referred to as the dielectric constant and the dielectric materials are the electrical insulators that get polarized when the external field is applied. When the dielectric material is embedded in between the parallel plate capacitor and an external electric field is applied, the material acquires positive and negative charge oriented in the opposite direction of the field applied, and polarization is thus induced. As the electric flux density is enhanced, the electrical polarization also increases, which further amplifies the dielectric constant, enabling it to store energy for a longer period.

The relative permittivity, another way to express dielectric constant, is symbolized by the kappa, κ, a Greek letter which is simply expressed as a ratio of material's capacitance (C) to that of capacitance showed in vacuum i.e. C_0 ($\kappa = C/C_0$). (Richerson and Lee 1992). It is a unitless number having no dimension. Materials having a high dielectric constant act as excellent capacitors and are applicable in other devices, like microelectronics. The material having a low dielectric constant is also demanded and used as an electrical insulator. Relative permittivity (κ) can also be expressed as

$$\kappa = \varepsilon' - j\varepsilon''$$

$$\kappa = \varepsilon_0\varepsilon_r - j\varepsilon'' \qquad (1.5)$$

In the above equation, ε' is the real dielectric constant, and ε'' is the imaginary dielectric constant. The real dielectric constant (ε') depends on the nature of the material, the frequency applied, the temperature at which data is collected, the magnitude of voltage, and time. The polarization due to all the above characteristics has

specific mechanisms(Koops 1951; Bai et al. 2000; Cohen et al. 2003; Kretly et al. 2003; Balamurugaraj et al. 2013).

The most extensively studied perovskite showing a fascinating dielectric constant is $CaCu_3Ti_4O_{12,}$ (CCTO), a complex perovskite oxide. This electro ceramic shows dielectric permittivity (ε) as high as 10^5. It is synthesized for varied applications, for instance, as a capacitor, memory devices, a sensor, a resonator or microelectronic devices, etc (Fang et al. 2004; Ferrarelli et al. 2006; Huijben et al. 2006; Huízar-Félix et al. 2012). These applications are an outcome of the properties accomplished by the unique structure of CCTO(Zhuk et al. 2018). The structure of $CaCu_3Ti_4O_{12}$ is derived from the cubic perovskite (ABO_3) represented by the general formula $AA'_3B_4O_{12}$ forming a cubic lattice, in which A and A' occupy corners, B are confined at body-centered, and oxygen occupies the face-center. The unique behavior in the material can be attributed to the structural variation in which the octahedral tilt distortion appears in the cubic lattice due to a mismatch in the nature and the size of the A cations. (Demmig-Adams and Adams 2006). Additionally, the TiO_6 octahedral tilt produced in the structure, where three-quarters of the A sites occupied by Cu^{2+} cations exhibit square–planar coordination and Jahn-Teller distortion. The remaining one-quarters of the A sites reside in Ca^{2+}, exhibiting 12-fold coordination. This unique structure provides the material its specific features and thus the demand for infinite tailoring opportunities around it.

1.11 Dielectric loss

Dielectric loss is the inherent property shown by the dielectric materials and it is actually the loss of energy, mostly in the form of heat due to constant fluctuation in the direction of polarization, given to the fact that an alternating electric field is applied. It should be noted that this is not a feature that is a factor of the geometry of the capacitor

or the dielectric material. It is also termed as Dissipation factor (D_f) or more commonly, loss angle (δ) or loss tangent ($tan\ \delta$). It refers to the specific phase of the complex plane, whose real as well as the imaginary parts exhibits resistive (lossy) component to its electromagnetic field where as the reactive (lossless) counterpart is better shown by the following equation

$$tan\ \delta = \varepsilon''\varepsilon' + \sigma 2\pi f \varepsilon \quad (1.6)$$

where, ε′ is the real part of dielectric permittivity and ε″ symbolizes the imaginary part of dielectric permittivity and f represents frequency, and σ is electrical conductivity shown by the materials. The reason for the tangent loss (tan δ) or the loss of energy in the dielectric materials is the dipolar and interfacial polarizations accompanied by distortion loss and conduction loss. Distortion loss comes in affect at higher frequency regions and is mainly governed by ionic as well as electronic polarization mechanisms. On the other hand, conduction loss is the consequence of the flow of actual positive and negative charges across the dielectric materials which are responsible for the D.C electrical conductivity in the materials. As stated earlier, the main reason for dielectric loss is because of the molecular or atomic rotation under the influence of alternating electric fields. The energy loss (W) caused by dielectric loss (tan δ) in the capacitor or the dielectric materials arises as a result of three factors, namely the D.C conductivity, Ionic vibration and the deformation loss, the ionic jumps during dipolar reorientation causing the relaxation losses (Shujahadeen et al. 2018). Loss of energy (W) within the dielectric materials can be evaluated using the following equation

$$W \approx \pi \varepsilon' \xi\, 2f\ tan\ \delta \quad (1.7)$$

Where f symbolizes frequency and ξ is used to denote the electric field strength. Therefore, for the longevity of the dielectric materials or to minimize the energy dissipation, and better performance at a higher frequency range, it is required to obtain

dielectric loss as low as possible. Generally, a dielectric material exhibits high dielectric loss when it is under 5% and low when it is around 0.1% [Ulrich and Schaper (2003)].

1.12 Impedance

Dielectric spectroscopy depending on the frequency is regarded as impedance spectroscopy (IS). Graphical representation of it is referred to as a form of Nyquist plot or Cole-Cole plot. This technique provides a platform for the accurate measurement of electrical properties of the materials over a broad range of frequencies, whether it is solid or liquid. Interaction of the external electric field with the electric dipole moment within the materials (often expressed by permittivity) provides the base of this spectroscopy. Impedance spectroscopy proves to be a quite useful technique to study the composite material as it is an interaction of external electric field which is alternating in nature. It has a significant effect on the electric dipole moment depending on interfaces (interfaces among different phases, grain boundaries, and the pores) (Gerhardt (1994)]. Data obtained from spectroscopy is employed to evaluate capacitance and loss tangent or real and imaginary impedance over a frequency range. The information about the presence of grains, grain boundaries and surface effects that influence electron transfer reaction can be obtained by utilizing the impedance spectroscopy technique. The high value of the dielectric constant of the materials is explained on the basis of the internal barrier layer capacitance (IBLC) mechanism (Leret et al. 2007). According to IBLC mechanism, materials possess grains separated through grain boundaries in which grains are semiconducting in nature whereas grain boundaries are insulating properties. The higher value of grain boundary resistance in comparison to that of grain resistance in the materials is responsible for the high dielectric constant because of larger difference in electrical conductivity of $CaCu_3Ti_4O_{12}$ (Chiodelli et al. 2004). A considerable difference in conductivity develops space charge polarization that is dominant in the lower

frequencies (hertz to kilohertz) at the barrier layer between grains and grain boundaries. This gap is the crucial factor for the giant dielectric constant of a wide variety of materials (Gerhardt and Nowick 1986, Ramanujachary *et al.* 1988, Cao *et.al.* 1990 and Kim. *et al.* 1997). In some cases, the semicircle of grains (bulk) or electrode that appears at a very high frequency is missing due to instrument limitations. After measuring Capacitance and tan δ with the help of LCR meter and measuring the current flow through the material in which L represents inductance, C represents capacitance and R represents resistance. All the parameters such as impedance *(Z*),* dielectric constant (ε*), electric modulus (*M**), and admittance (Y*) can be measured. These functions are in turn related to one another as follows (Gerhardt et al.1994).

$$\varepsilon^* = \varepsilon' - j\,\varepsilon'' \tag{1.8}$$

$$Z^* = \frac{1}{R_g^{-1} + i\omega C_g} + \frac{1}{R_{gb}^{-1} + i\omega C_{gb}} = Z' - iZ'' \tag{1.9}$$

Where

$$Z' = \frac{R_g}{1+(\omega R_g C_g)^2} + \frac{R_{gb}}{1+(\omega R_{gb} C_{gb})^2}$$

And

$$Z'' = R_g\left[\frac{\omega R_g C_g}{1+(\omega R_g C_g)^2}\right] + R_{gb}\left[\frac{\omega R_{gb} C_{gb}}{1+(\omega R_{gb} C_{gb})^2}\right]$$

Z^*, Z' *and* Z'' represents complex, real and imaginary impedance, whereas R_g and C_g are resistance and capacitance of grains, R_{gb} and C_{gb} are the resistance and capacitance of grain boundary. $\omega = 2\Pi f$, f indicate frequency

and $$\tan\delta = \frac{\varepsilon''}{\varepsilon'} = \frac{Z'}{Z''} \tag{1.10}$$

Since these functions are interrelated, only one set of measurements is needed to calculate all of them (Macdonald 1987 and Gerhardt 1994). Studying dielectric data in the different functions allows different features to be recognized.

Three different basic regions for the exchange interactions between current and sample

(a) Within the grains.

(b) The grain boundaries.

(c) Electrodes surfaces.

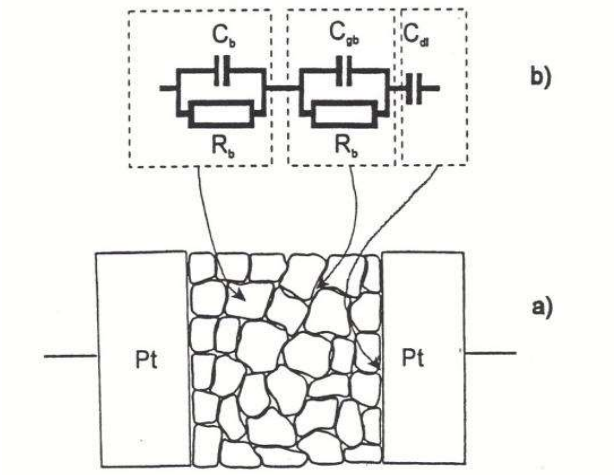

Figure 1.11 Complex plot of impedance plane and its equivalent circuit

1.13 Ferroelectricity

Ferroelectricity is the property of the material existing in single or polycrystalline form exhibiting reversible spontaneous polarization over a certain range of temperature, that can be reversed in direction by the application of an appropriate electric field. This type of material was discovered in 1920 in Rochelle salt by Valasek. The phenomenon of the ferroelectric in the materials can be explained on the basis of the hysteresis loop, shown in figure1.11.

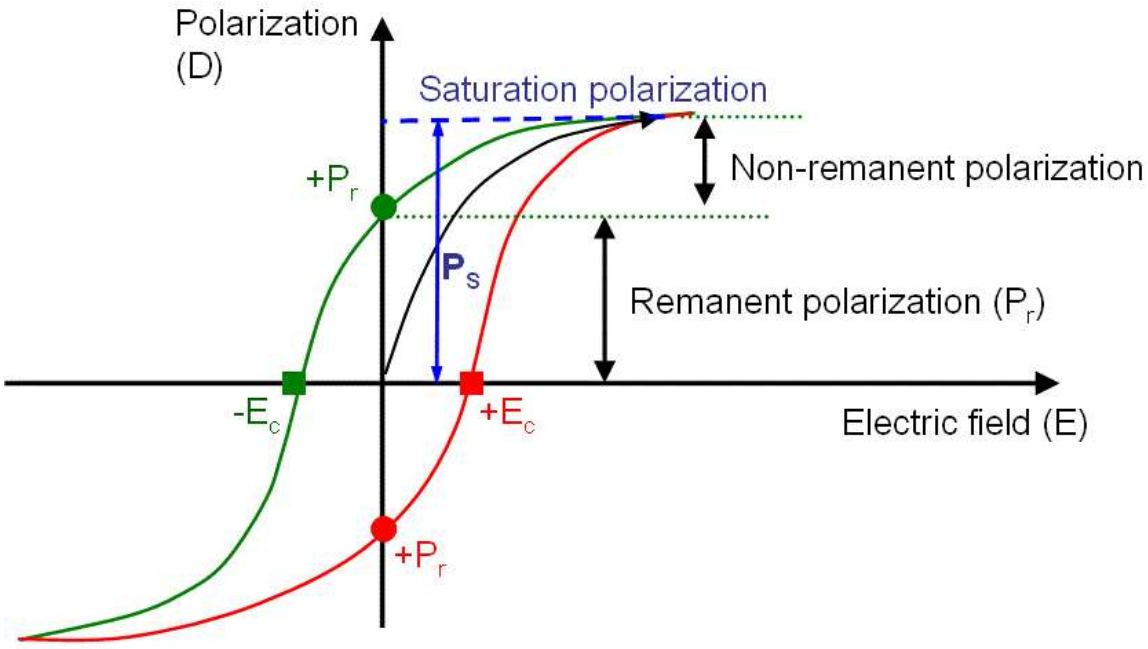

Figure 1.12 PE hysteresis loop

The remanent polarization and coercive field were measured with the help of polarization versus electric field variation, for which saturation polarization must be present in the P-E hysteresis loop. The presence of polarization in the materials in the absence of an external electric field (E=0) is called remanent polarization, whereas the value of the field at zero polarization is called coercivity field (Ghosh et al. 2016). A number of materials with perovskite (ABO_3) type structure that exhibits ferroelectricity, such as KH_2PO_4 (KDP), $LiTaO_3$ (LT), $PbTiO_3$ (PT), $Pb(Zr,Ti)O_3$ (PZT), $NH_4H_2PO_4$ (ADP), $LiNbO_3$ (LN), $BaTiO_3$ (BT), $(Pb,La)(Zr,Ti)O_3$ (PLZT), and $(Pb,La)TiO_3$ (PLT) were discovered. The unusual dielectric constant observed in the $BaTiO_3$ (BT) is due to the displacement of atoms from their original lattice point in the particular orientation and attained non-centrosymmetric structure resulting in spontaneous polarization. Below the certain temperature called curie temperature (Tc), ferroelectricity is observed in the materials, however their ferroelectricity disappears

above this temperature and the transition of the ferroelectric phase in to the paraelectric phase or transition order-disorder phase having higher symmetry than earlier.

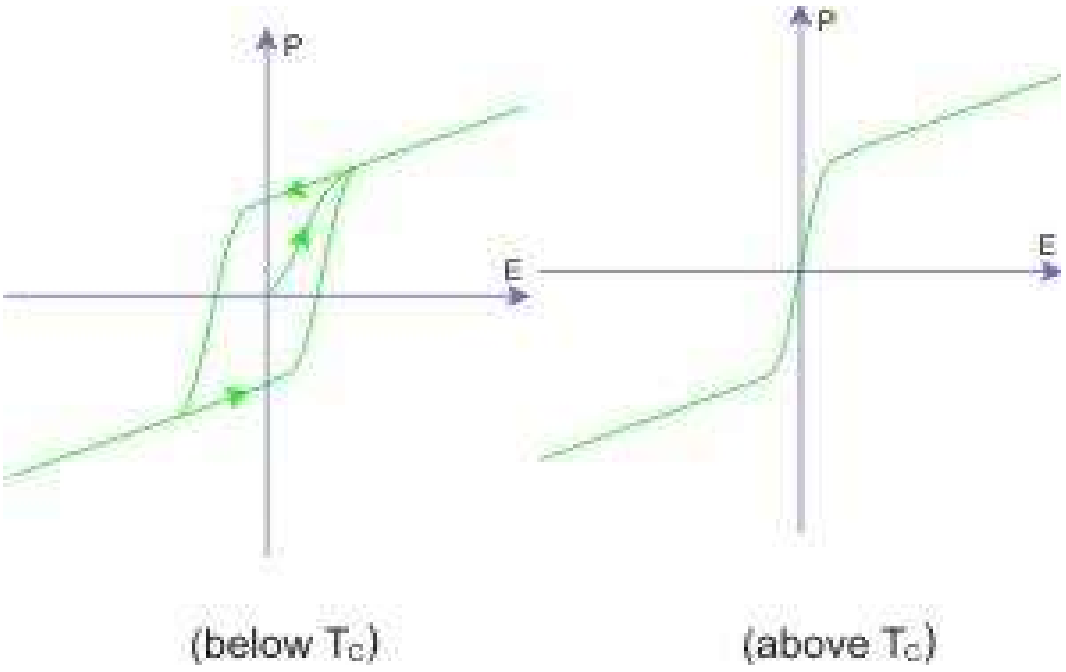

Figure 1.13 P-E hysteresis loops for $BaTiO_3$ above and below the Curie temperature (Tc)

For example, the transformation of low symmetry tetragonal $BaTiO_3$ to higher symmetry cubic $BaTiO_3$ at about 120°C while heating. The term paraelectric involves in centrosymmetric suggests an analogy with paramagnetism where the dipoles are randomly oriented in the crystal that is why polarization becomes zero. Therefore, materials must be non-centrosymmetric for the existing ferroelectricity phenomenon which indicates that mechanical strain caused by phase transition will change not only the shape and volume of the materials but also change their refractive index. Hence, ferroelectric materials exhibit not only ferroelectric phenomena but also pyroelectric, electro-optic effects, and piezoelectric, which can be used for many technological applications such as light deflectors, displays and other electro-optic devices (Qi *et al*., 2002).

1.14 Magnetic Properties

Magnetism is defined as an attractive and repulsive phenomenon exhibited by any material. It is a material attribute that results from the alignment of magnetic moments. A magnetic field is generated by the net flow of electric charge and magnetic moments of constituting particles of the material, which act on nearby magnetic moments as well as currents. In the presence of an external magnetic field, the electronic spins present in the materials align themselves, altering the magnetic field strength (Koehler and Wollan 1957; Rajeswari et al. 1998; Roy et al. 2005; He et al. 2010; Andres et al. 2012 Jan 1; Markovich et al. 2014). This change in the magnetic field is referred as magnetization (M). The magnetic flux density shown by the materials (denoted as B) is expressed by the equation

$$B=\mu_0 H+\mu_0 M \tag{1.11}$$

In the above equation, μ_0 is called the universal constant as the permeability of free space ($4\pi \times 10^{-7}$ H/m), H is the symbol for magnetic field strength and M represents magnetization. Magnetization in other words, the net magnetic moment per unit volume of a substance, is defined as

$$M= \chi_m H \tag{1.12}$$

Where χ_m is a mathematical symbol denoting magnetic susceptibility and

$$\chi_m= \mu_r-1 \tag{1.13}$$

Table 1.6 The high dielectric constant of few oxides compound

S.No.	Compound	Dielectric constant	Reference
1.	$CaCu_2Mn_1Ti_4O_{12}$	5×10^3	(V. Kumar et al. 2020)
2.	$Bi_{2/3}Cu_3Ti_4O_{12}$	2.9×10^4	(Gautam et al. 2016)
3.	$Y_{2/3}Cu_3Ti_4O_{12}$	8434	(Sharma et al. 2014)
4.	$Y_{2/3}Cu_{2.90}Zn_{0.1}Ti_4O_{12}$	1.85×10^4	(Sharma et al. 2018: 2)
5.	$CaCu_3Ti_4O_{12}$	10^4	(V. Kumar et al. 2020)
6.	$BaFe_{11.95}Co_{0.05}O_{19}$	2.3×10^3	(A. Kumar et al. 2020)
7.	$CaCu_3Ti_{4-x}Sn_xO_{12}$	6.51×10^4	(Boonlakhorn and Thongbai 2020)
8.	$0.5Bi_{2/3}Cu_3Ti_4O_{12}$ - $0.5Bi_3LaTi_3O_{12}$	13.94×10^3	(Gautam et al. 2017)
9.	$Ba_6Y_2Ti_4O_{17}$	1.5×10^3	(Yadava et al. 2016)
10.	Eu_2CuO_4	5×10^3	(Salame et al. 2014)
11.	$Bi_4Ti_3O_{12}$-$BaTiO_3$	4.75×10^3	(Singh *et al.* 2020)
12.	$CaCu_{2.9}Zn_{0.1}Ti_4O_{12}$	5971	(Singh et al. 2013)
13.	$Y_{2/3}Cu_3Ti_{3.95}In_{0.05}O_{12}$	5068	(Singh *et al.*2016)
14	$Bi_{0.5}Na_{0.5}TiO_3$	5000	(Lin *et al.* 2004)
15.	$(Ba_{0.95}Ca_{0.05})$ $(Ti_{0.96}Zr_{0.04})O_3$	3910	(Yang et al. 2011)
16.	$SrTiO_3$	2150	(Penn et al. 1997)
17.	$Bi_4Ti_3O_{12}$	1400	(Xiang et al. 2006)

Where, $\mu_r = \mu / \mu_0$ (1.14)

Here in equation 1.13, μ_r is the symbol for relative permeability. As expressed in equation 1.14, relative permeability μ_r is the ratio of permeability of the material (μ) to the permeability of free space (μ_0). The degree or extent to which a material can be magnetized is measured by this ratio. Applications of magnetic materials can be seen in a variety of appliances, a few of them are microwave devices, magnetic recording media, data storage tunnel junction, video recorders, etc. (Hamid et al. 2006). Physical properties such as magnetic coupling, high electrical resistivity and low loss are associated with the magnetic materials. As per requirement, these properties can be altered by altering the structure and composition. Along with-it magnetic behavior is much affected by the particle size, morphology, chemical composition as well as synthetic routes. However, it should be pointed out that if the particle size is below 100 nm, the concentration of atoms on the surface will be high. Thus, even by changing the structure in the nanoscale, magnetic properties can be changed (Richerson and Lee 1992; Chu et al. 2002; Chaudhuri and Mandal 2012).

1.14.1 Origin of magnetism

The origin of magnetism in a material lies in the motion of negatively charged electrons. The overall magnetic moment is the resultant of the magnetic moment generated by the spin motion of electrons around its axis and the orbital motion of electrons around the nucleus. The former referred as spin magnetic motion (μ_s) and later referred to as orbital magnetic motion (μ_l). However, they may or may not be magnetic. The magnetic quantum number (Ms) values are either +1/2 or -1/2, which signifies the direction and the value of the spin of an electron. When two electrons are paired in the orbital, their spin motion is equal and opposite, thus, magnetic moments cancel out each other,

causing a very weak magnetic field. However, the material exhibits considerate magnetic behavior when the electrons in the orbitals are unpaired. Transition metals have a higher tendency of being magnetic as they possess unpaired electrons in their d orbitals.

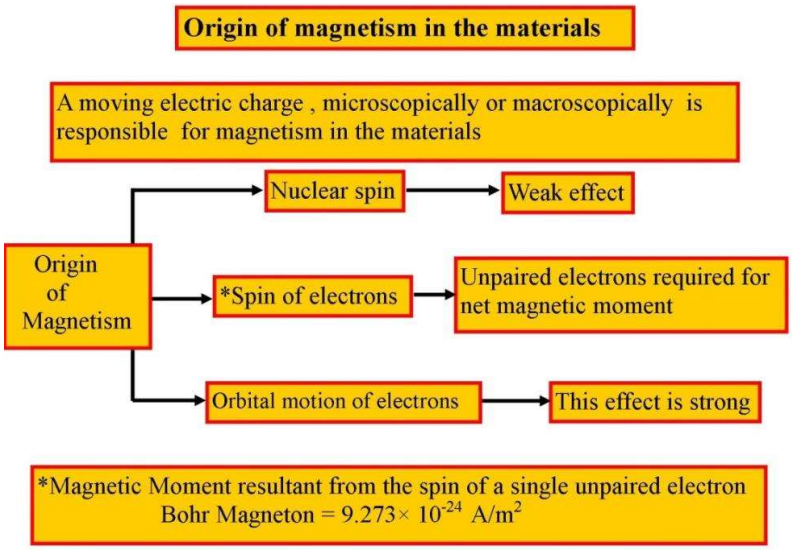

Figure 1.14 Flow chart for the origin of magnetism in the materials.

1.14.2 Magnetic Domain

Magnetic domains are a small region within the magnetic material, where all magnetization happens to be in a uniform direction. It should be noted that in material, the magnetic moment (or spin of the electron) of all the atoms in a region are arbitrarily oriented. In the magnetic domains at a certain area, approximately billions of atoms are found in a millimetre size. In the absence of a magnetic field, the spinning of electrons in ferromagnetic materials is random, resulting in a soft substance. In the case of ferromagnetic material magnetized easily, but no time of period retain (Chu et al. 2002; Chaudhuri and Mandal 2012). In the presence of a magnetic field, the magnetic domains are aligned parallel in the same direction. As a result, the material's net magnetic moment is non-zero and exhibits high magnetization. These materials are hard and have

Table 1.7 Various types of magnetic behavior at glance.

Types of magnetism	Susceptibility	Atomic/Magnetic behaviors		Example
Diamagnetism	Small & negative, -10^{-6} to 1	Atoms have no magnetic moments	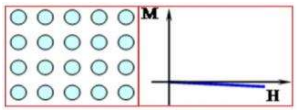	Au, Cu, Hg etc.
Paramagnetism	Small & positive, $+10^{-5}$ to $+10^{-3}0^{-5}$	Atoms have randomly oriented magnetic moments	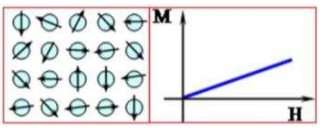	O_2, NO B_2,etc.
Anti-ferromagnetism	Small & Positive $+10^{-5}$ to $+10^{-3}$	Atoms have mixed parallel and anti parallel aligned magnetic moments	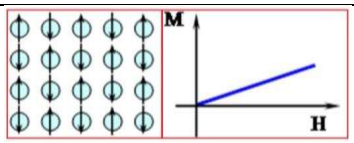	Mn, Cr, MnO, NiO etc.
Ferrimagnetism	Large & positive (~3) (below Tc), Function of applied field, Microstructure dependent	Atoms have anti-parallel aligned magnetic moments	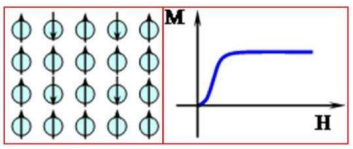	Ba ferrite
Ferromagnetism	Large & positive (below Tc), Function of applied field, Microstructure dependent	Atoms have parallel aligned magnetic moments	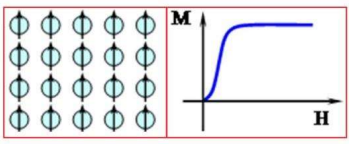	Fe, H, Co, Ni etc.

a permanent magnetic moment, which means that their magnetization continues even when the magnetic field is removed (Zhao et al. 2004; Andres et al. 2012 Jan 1).

The first person to classify chemical substances on the basis of their magnetic properties was Michael Faraday in the nineteenth century. Faraday's distinction basis was the force experienced by the materials when an external inhomogeneous magnetic field was applied to them. All the category of magnetism is shown in table 1.7.

1.14.3 Hysteresis loop

Magnetic characteristics of the material can be determined by studying the relationship of the magnetizing force (H) with the induced magnetic flux density (B). The plot of this relationship is referred as the B-H curve, also termed the hysteresis loop. A typical hysteresis loop of a ferromagnetic materials is illustrated in figure 1.15.

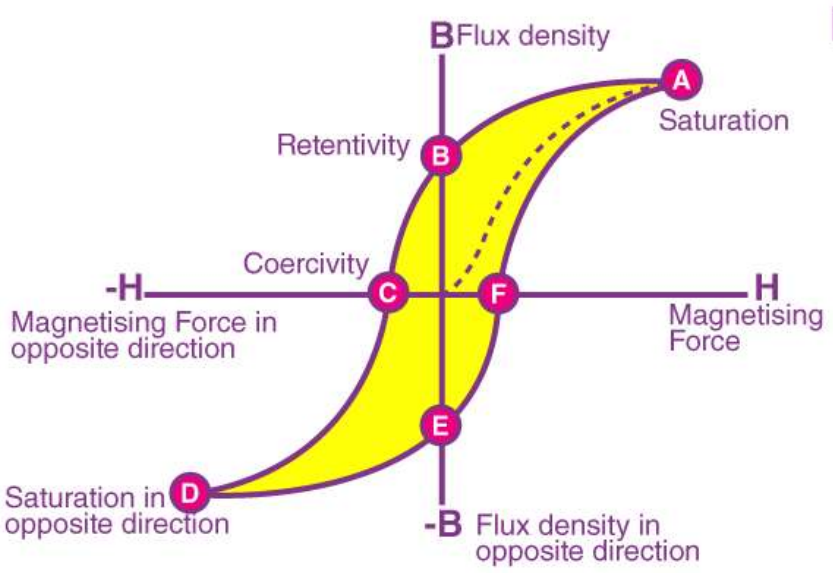

Figure 1.15 Hysteresis loop or B-H curve

When an external magnetizing field is applied to a ferromagnetic material, such as nickel, cobalt, or iron, alignment of the atomic domains occurs, and once aligned magnetic property is developed in the material, that remains conserved eternally even if

the external magnetizing field is removed. If it is needed to demagnetize the material, an external magnetizing field in the reverse direction must be applied (Makar and Tanner 1998).

The parameters required to define a magnetic material that can be evaluated from the hysteresis loop are provided below (Goll 2007).

(i) **Retentivity –**A degree of the residual flux density at the saturation induction in the magnetic material. it measures the ability of the material to retain a finite magnitude of the residual magnetic field when the external magnetizing force is eliminated after reaching saturation, represented by point B on the hysteresis curve.

(ii) **Residual Magnetism** or **Residual Flux -** some of the magnetic domains retain a degree of orientation relative to the magnetic field that was applied to the core. This phenomenon is known as residual magnetism. The magnetic flux density that remains a material when the magnetizing force is zero. It is remarked that both retentivity and residual flux density have the same value when the material has been magnetized to the saturation point. It is observed that when the magnetizing force does not attain the saturation level, the level of retentivity may be greater than the value of residual magnetism.

(iii) **Coercive Force –** The magnitude of the magnetic field required in the opposite direction to return the value of magnetic flux to zero.

(iv) **Permeability –** The ease with which a material can generate magnetic flux in its component is referred to as its permeability.

(v) Reluctance - the resistance that a ferromagnetic material displays to the creation of an internal magnetic field. The resistance offered by the electrical circuit is analogous to reluctance.

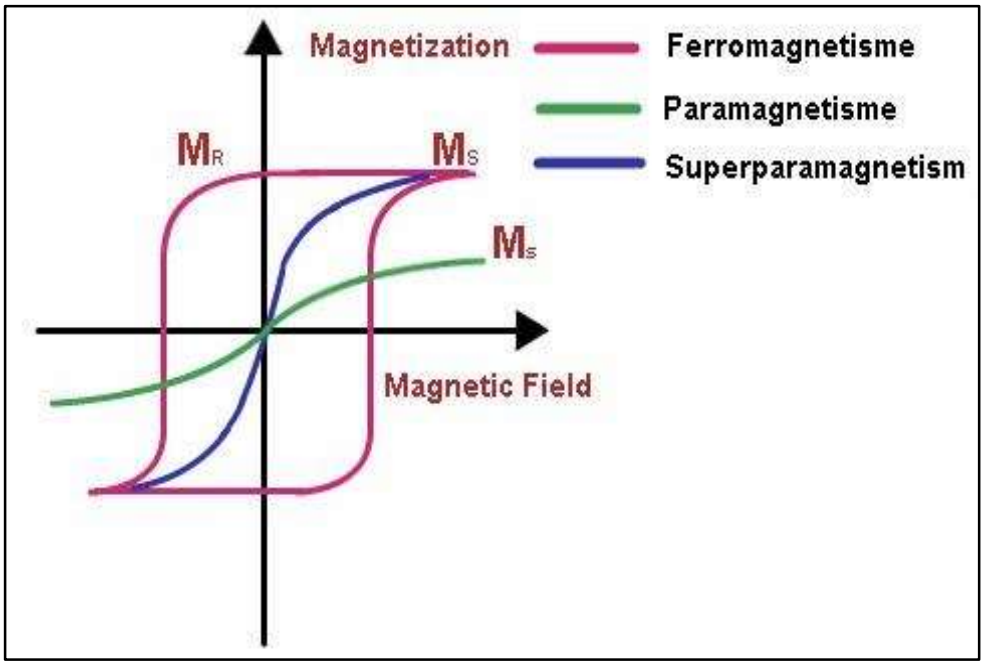

Figure 1.16 shows the M-H hysteresis curve for paramagnetism, superparamagnetism, and ferromagnetism.

1.15 Dye Degradation an Overview

Heterogeneous photocatalysis has been an extensively pursued research study for over the last two decades, which is widely applied for the degradation of the dyes. In the materialistic world of today, the demand depends on the outer appearance of products like leather, clothes, plastic products, accessories, or furniture, and for coloring these products, synthetic dye is needed. Unfortunately, in the process of dyeing, approximately 20% of the dye is lost as waste and enters the environment (Naresh and Mandal 2014). Subsequently, a substantial amount of synthetic dyes is released as wastewater discarded from the industry. Thus, to ensure a constant supply of clean water, recycling and reclaiming wastewater is a must. Conventional methods of

reclaiming water chemically, physically or biologically have been applied excessively for treating waste water having synthetic dye molecules. However, these processes have some drawbacks, such as the requirement of high energy, cost-ineffective as well as in the treatment process generates secondary pollutants (Barlow 1999).

However, Photocatalytic degradation of pollutants in wastewater is one of the efficient and inexpensive methods leading to complete deterioration into non-toxic molecules such as water and carbon dioxide. In this process mainly electrons are transferred to the conduction band from the valence band of a material surface (mostly chalcogenides) on irradiation with solar light of appropriate wavelength (Kong et al. 2019)This phenomenon generates excitons which react with oxygen or water molecules to produce hydroxide radicals and superoxide anions. The latter species exhibits a very high oxidizing tendency which can degrade a wide variety of organic pollutants, including synthetic dyes. This decontamination method via these reactive species comes under the forms of Fenton processes, also termed as Advanced Oxidation Process (AOP) (Rana et al. 2005).

The photocatalyst that is exhaustively studied for the photocatalytic degradation of dye is titanium dioxide, but its efficiency is yet to reach. TiO_2 has three prominent phases, namely Bookite, Rutile and Anatase, among which the anatase form of TiO_2 have reported to display higher photon absorption characteristics due to the triangular arrangement of the oxygen ions on the surface of anatase, allowing considerable adsorption of organic pollutants, along with in the anatase phase, the orientation of titanium ions favors reactions with the adsorbed molecules. Intriguingly, small proportion of rutile phase present in pure anatase has proved to be favorable for the adsorption of dye even though the former lacks the favorable arrangements of the ions.

The reason of it can be attributed to mesoporosity in the structure of the rutile phase (Viswanathan 2018).

The intensity of exposed light is another deciding factor that governs the percentage dye degradation in the waste water. The process of recombination of the excitons has an inverse effect with the intensity of irradiation, at higher intensity of irradiation, the recombination process slows down, on the contrary at low intensity, the electron hole recombination predominates (Sunkara and Misra 2008; Venkatasubramanian et al. 2008).

The crucial parameter deciding the efficiency of photocatalytic activity is the band gap of the material. Band gap helps in resolving the appropriate wavelength of solar radiation required for the catalytic activity (Huijben et al. 2006).

Primarily photo assisted degradation is still limited by the wide bandgap, which shows UV light responsive characteristics. The UV-responsive single metal oxide photocatalysts are categorized as first-generation photocatalysts. But lately, there has been a need to develop photocatalytic materials that are responsive to visible light irradiation. Thus, the latest research is devoted toward designing photocatalysts with minimum bandgap, responsive in the visible region, and categorized as second-generation photocatalysts. Moving towards the aim of shifting the irradiation wavelength in the visible light range, modification in the structure of already existing photocatalysts or coupling photocatalysts to reduce band gap is needed (Lachheb et al. 2002).

1.15.1 Mechanism of Photocatalytic Dyes Degradation

The main steps involved in the mechanism of photocatalytic degradation of dyes through the radical species formed due to photoexcitation of the photocatalyst are expressed in the following steps.

Photoexcitation:

$$\text{Photocatalyst} + \text{photons (hv)} \rightarrow e^- (CB) + h^+ (VB) \quad (1.15)$$

Charge-carrier trapping of e^-:

$$e^- (CB) \rightarrow e^- (tr) \quad (1.16)$$

Charge-carrier trapping of h^+:

$$h^+ (VB) \rightarrow h^+ (tr) \quad (1.17)$$

Electron–hole recombination:

$$[e^- (tr)] + [h^+ (VB) + h^+ (tr)] \rightarrow \text{heat} \quad (1.18)$$

Oxidation of hydroxyls:

$$OH^- + h^+ \rightarrow \bullet OH \quad (1.18)$$

Photogenerated e^- scavenging:

$$(O_2)_{ads} + e^- \rightarrow O_2^{\bullet -} \quad (1.20)$$

$$O_2^{\bullet -} + e^- \rightarrow HOO\bullet \quad (1.21)$$

Photodegradation of organic by •OH:

$$\text{Organics} + \bullet OH \rightarrow CO_2 + H_2O \quad (1.22)$$

Photodegradation of organic by h+:

$$\text{Organics} + h^+ \rightarrow CO_2 + H_2O \quad (1.23)$$

Photodegradation of organic by $O_2^{\bullet -}$ / HOO•:

$$\text{Organics} + O_2^{\bullet -} / HOO\bullet \rightarrow CO_2 + H_2O \quad (1.24)$$

Here, e^- (tr) denotes the surface-trapped VB electron and h^+ (tr) is the surface-trapped CB hole, $O_2^{\bullet -}$ is the superoxide radical and hydroperoxyl radical is represented as HOO•. As expressed in equation (1.17), the recombination of photogenerated e^- with h^+ occurs in nanoseconds (ns) with simultaneous heat energy dissipation, thus for an efficient photocatalytic degradation, this step is prevented (Viswanathan 2018; Kong et al. 2019).

\

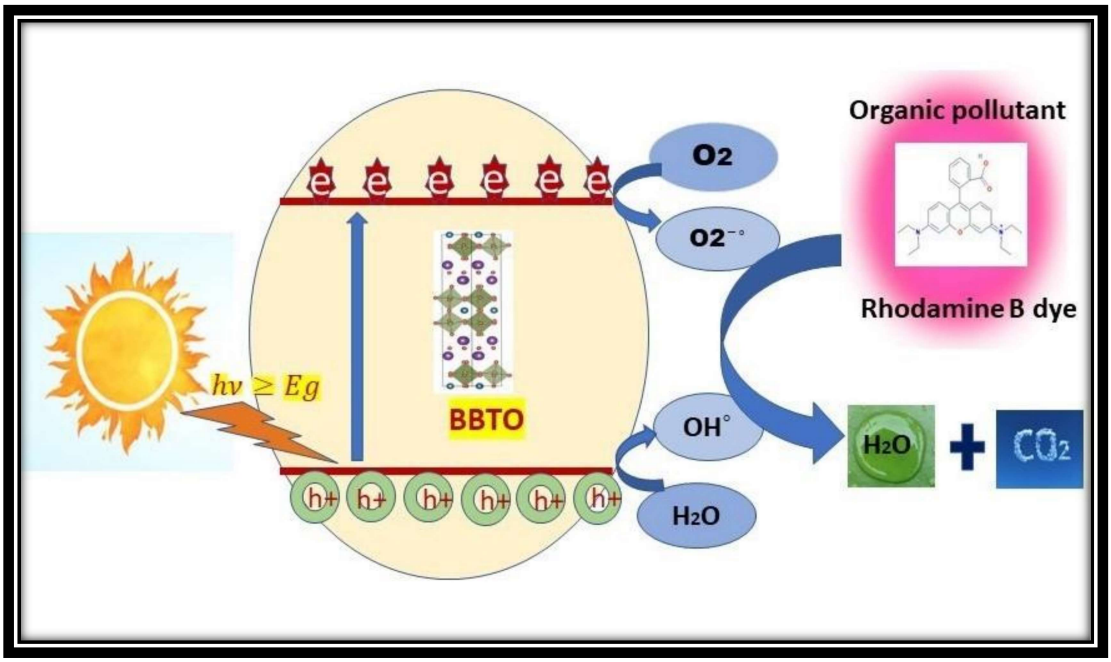

Figure 1.17 The pictorial representation of Photocatalytic Dyes Degradation.

1.15.2 Photocatalysts used in Dyes Degradation

A wide variety of photocatalysts have been synthesized and employed to date, however, within the perovskite-related family, it is observed that as compared to bulk non-layered perovskite photocatalysts, layered perovskite-related photocatalysts are better suited for the separation as well as diffusion of photogenerated electron-hole pairs.

The most prominent layered perovskites, as already discussed earlier, are namely the Ruddlesden-Popper phases having the general formula $A_{n+1}B_nO_{3n+1}$ (e.g., $Li_2CaTa_2O_7$), the Dion-Jacobson phases given by general formula $A_{n-1}B_nO_{3n+1}$ (e.g., $RbLaNb_2O_7$), and the Aurivillius phases having the general formula $((A_{n-1}B_nO_{3n+1})^{2-}(A_2O_2)^{2+})$. Here, in all three cases, n denotes the number of layers of the perovskite structure. According to the reported work, it is established that among these

layered perovskite-related family, Aurivillius phases exhibits the most promising results in photocatalytic activity (Hwang et al. 2017).

The Aurivillius phases have unique intergrowth structures constituted of alternating layers of $(Bi_2O_2)^{2+}$) units with perovskite-related ($(A_{n-1}B_nO_{3n+1})^{2-}$) blocks. The alternating layered arrangement, along with providing better polarization of charge species, also provides a better possibility for the diffusion and separation of the photoexcited hole–electron pairs compared to other non-layered photocatalysts (Naresh and Mandal 2014). The separation is possible as the reduction and oxidation lattice sites reside in an isolated manner on the edges and faces of the unit ultrathin sheets. The holes generated in the layered photocatalysts are trapped by water molecules present in the interlayer while diffusing to the sheet surface. This accelerated trapping method of holes causes electrons to be easily and efficiently diffused within the unit sheets before getting to the edges of the sheets (Liu et al. 2014). Additionally, bismuth (Bi) is a p-block element with filled d orbital, and s-orbital of the valence shell (Bi 6s) can hybridize with p-orbital of oxygen (O 2p) generating hybridized valence band (VB), which facilitate the mobility of holes in the VB generated by the photons and improves the photocatalytic efficiency of the Aurivillius oxide (Zhang et al. 2011 May).

$Bi_4Ti_3O_{12}$, a parent Aurivillius oxide (where n = 3) is well explored as a visible-light-driven photocatalyst in all forms such as $Bi_4Ti_3O_{12}$ films, $Bi_4Ti_3O_{12}$ particulates and even in platelets form (Hou et al. 2013: 1). Regrettably, individual phase of $Bi_4Ti_3O_{12}$ nanomaterials shows low photocatalytic efficiency due to fast rate of electron–hole pairs recombination. As discussed above, to reduce the band gap or in other words to increase light harvesting property, coupling of photocatalysts or hybrid photocatalysts is preferred over one individual photocatalyst. This hybrid photocatalysts displays synergistic effects of the each species, providing prolonged carriers lifetime, better

chemical stability and enhanced catalytic performance (Venkatasubramanian et al. 2008).

1.16 Aim of the present work

This aim is mainly focused on the crystal structure analysis of Aurivillius oxides. The structural distortions and the driving force behind them will be discussed. The cation doping effects, site mixing between cations inside the perovskite block and Bi ion in the bismuth oxide layer, as well as the perovskite layer effect, will be studied to investigate the trend for structural features. The structural features tracked here primarily direct to the local environments around Ti and the interface between perovskite block and bismuth oxide layer. The second major part is aimed at linking the crystal structure features with their electrical and magnetic properties. So, the material properties can be optimized with careful control of crystal structures from different compositions.

Barium Titanate $Bi_4Ti_3O_{12}$ is one best-known typical compounds of Aurivillius oxides owing to its credible application in ferroelectric memories and optical devices and it has been intensively studied as a photocatalyst for water splitting and for degradation of organic pollutants. Regrettably, the conductivity of $Bi_4Ti_3O_{12}$ hinders the polarization and low photocatalytic efficiency of individual phase $Bi_4Ti_3O_{12}$ nanomaterials is obtained due to the rapid recombination of photoexcited electron-hole pairs (Liu et al. 2014). Thus, to improve the polling processes by structural modification, various other perovskites have been added. $BaTiO_3$, one such perovskite with colossal polarization spawning excellent ferroelectric and dielectric properties, is opted to add in $Bi_4Ti_3O_{12}$ to yield a new ceramic material $Bi_4BaTi_4O_{15}$ (BBTO) in the present work. BBTO belongs to the Aurivillius family where m = 4, which suggests it is

even layered and thus, polarization only exists in the a-b-axis and missing along the c-axis. A-site in the perovskite is occupied by Ba and Bi ion while B-site by Ti ion. Due to its peculiar crystal structure, BBTO exhibits anisotropic ferroelectricity and novel electrical properties and with increased light harvesting, the prolonged lifetime of carriers enhances catalytic performance as well as higher chemical stability.

(i) The thesis focuses on the synthesis and characterization of ceramic materials, as well as various types of applications such as dielectric and magnetic characteristics.

(ii) Grain and grain boundaries, morphological structure, particle analysis, temperature and frequency influence on dielectric and electrical characteristics have been investigated extensively.

(iii) This work deals with the method of synthesis of Bismuth Layered Aurivillius oxides and some experimental procedures carried on these ceramic materials. In general ceramic materials are hard and brittle, shows immense stability due to its inherent quality of being heat and corrosion resistive. Their interesting properties are further enhanced by employing different compositions and synthetic routes. Purity of the synthesized materials is of utmost importance; hence single-phase formation of the materials was controlled by reaction conditions and sintering temperature. Characterization of synthesized materials to obtain information regarding microstructure and particle size were obtained using various physicochemical techniques. Few physical properties such as dielectric, impedance, magnetic and hetero-photocatalytic were investigated too at a few selected temperatures and frequencies. In the present work, following Bismuth Layered Aurivillius oxides were synthesized.

i. $Bi_4Ti_3O_{12}$-$BaTiO_3$ (BTO-BT) by modified solid-state route
ii. $Bi_4BaTi_4O_{15}$ (BBTO) by chemical route
iii. $Bi_4SrTi_4O_{15}$ (BSTO) by chemical route

Different types of physiochemical characterization of the following above materials in the sequential steps:

I. X-ray powder diffraction (XRD) study was used for the identification of phase formation and the crystal structure of the materials.

II. Scanning electron microscope (SEM) analysis has been performed for the detailed morphological study of the fractured surface of the materials.

III. Transmission Electron Microscopy (TEM) is useful for particle size determination.

IV. The dielectric properties, dependent on both temperature as well as frequency, have been investigated.

V. The magnetic properties of the ceramics studied.

VI. The thermal behavior of the ceramic was studied with the help of Thermogravimetric analysis (TGA).

VII. The oxidation state of the element was to be examined with the help of X-ray Photoelectron Spectroscopy (XPS).

VIII. Metal oxygen bond was to be examined with the help of FT-IR.

IX. Grain and grain boundaries were also studied with the help of Raman spectroscopy.

1.17 References

Ali R, Yashima M. 2005. Space group and crystal structure of the Perovskite CaTiO3 from 296 to 1720K. Journal of Solid State Chemistry. 178(9):2867–2872. doi:10.1016/j.jssc.2005.06.027.

Allison M. 2007. Metrology and analysis of nano-particulate barium titanate dielectric material. Kansas State University. [accessed 2021 Jul 9]. https://krex.k-state.edu/dspace/handle/2097/529.

Amow G, Au J, Davidson I. 2006. Synthesis and characterization of La4Ni3−xCoxO10±δ (0.0≤x≤3.0, Δx=0.2) for solid oxide fuel cell cathodes. Solid State Ionics. 177(19):1837–1841. doi:10.1016/j.ssi.2006.01.017.

Andres J, Longo V, Cavalcante L, Moreira ML, Varela J, Longo E. 2012 Jan 1. A fresh look at the structural, ferroelectric and photoluminescent properties in perovskites. Photoluminescence: Applications, Types and Efficacy.:119–161.

Bai Y, Cheng Z-Y, Bharti V, Xu HS, Zhang QM. 2000. High-dielectric-constant ceramic-powder polymer composites. Appl Phys Lett. 76(25):3804–3806. doi:10.1063/1.126787.

Balamurugaraj P, Suresh S, Koteeswari P, Mani P. 2013. Growth, optical, mechanical, dielectric and photoconductivity properties of L-proline succinate NLO single crystal. J Mater Phys Chem. 1(1):4–8.

Barlow M. 1999. World Rivers Review. International Rivers Network, Berkeley.:6–7.

Boonlakhorn J, Thongbai P. 2020. Dielectric properties, nonlinear electrical response and microstructural evolution of CaCu3Ti4-xSnxO12 ceramics prepared by a double ball-milling process. Ceramics International. 46(4):4952–4958. doi:10.1016/j.ceramint.2019.10.233.

Cabuk S, Akkus H, Mamedov AM. 2007. Electronic and optical properties of KTaO3: Ab initio calculation. Physica B: Condensed Matter. 394(1):81–85. doi:10.1016/j.physb.2007.02.012.

Cain MG, Stewart M. 2014. Losses in Piezoelectrics via Complex Resonance Analysis. In: Cain MG, editor. Characterisation of Ferroelectric Bulk Materials and Thin Films. Dordrecht: Springer Netherlands. (Springer Series in Measurement Science and Technology). p. 233–242. [accessed 2021 Jul 11]. https://doi.org/10.1007/978-1-4020-9311-1_10.

Carrasco J, Illas F, Lopez N, Kotomin EA, Zhukovskii YF, Evarestov RA, Mastrikov YA, Piskunov S, Maier J. 2006. First-principles calculations of the atomic and electronic structure of F centers in the bulk and on the (001) surface of Sr Ti O 3. Physical Review B. 73(6):064106.

Chandler CD, Roger Christophe, Hampden-Smith MJ. 1993. Chemical aspects of solution routes to perovskite-phase mixed-metal oxides from metal-organic precursors. Chem Rev. 93(3):1205–1241. doi:10.1021/cr00019a015.

Chaudhuri A, Mandal K. 2012. Enhancement of ferromagnetic and dielectric properties of lanthanum doped bismuth ferrite nanostructures. Materials Research Bulletin. 47(4):1057–1061.

Chu M-W, Ganne M, Caldes MT, Brohan L. 2002. X-ray photoelectron spectroscopy and high resolution electron microscopy studies of Aurivillius compounds: Bi 4- x La x Ti 3 O 12 (x= 0, 0.5, 0.75, 1.0, 1.5, and 2.0). Journal of applied physics. 91(5):3178–3187.

Cohen MH, Neaton JB, He L, Vanderbilt D. 2003. Extrinsic models for the dielectric response of CaCu3Ti4O12. Journal of Applied Physics. 94(5):3299–3306. doi:10.1063/1.1595708.

Demmig-Adams B, Adams WW. 2006. Photoprotection in an ecological context: the remarkable complexity of thermal energy dissipation. New Phytologist. 172(1):11–21. doi:10.1111/j.1469-8137.2006.01835.x.

Dion M, Ganne M, Tournoux M. 1981. Nouvelles familles de phases MIMII2Nb3O10 a feuillets “perovskites.” Materials Research Bulletin. 16(11):1429–1435. doi:10.1016/0025-5408(81)90063-5.

Dubey AK, Singh P, Singh S, Kumar D, Parkash O. 2011. Charge compensation, electrical and dielectric behavior of lanthanum doped CaCu3Ti4O12. Journal of Alloys and Compounds. 509(9):3899–3906. doi:10.1016/j.jallcom.2010.12.156.

Ezhilvalavan S, Tseng T-Y. 2000. Progress in the developments of (Ba,Sr)TiO3 (BST) thin films for Gigabit era DRAMs. Materials Chemistry and Physics. 65(3):227–248. doi:10.1016/S0254-0584(00)00253-4.

Fang L, Shen M, Cao W. 2004. Effects of postanneal conditions on the dielectric properties of CaCu3Ti4O12 thin films prepared on Pt/Ti/SiO2/Si substrates. Journal of Applied Physics. 95(11):6483–6485. doi:10.1063/1.1728308.

Ferrarelli MC, Adams TB, Feteira A, Sinclair DC, West AR. 2006. High intrinsic permittivity in Na1⁄2Bi1⁄2Cu3Ti4O12. Appl Phys Lett. 89(21):212904. doi:10.1063/1.2388251.

García-Landa B, Ritter C, Ibarra MR, Blasco J, Algarabel PA, Mahendiran R, García J. 1999. Magnetic and magnetotransport properties of the ordered perovskite Sr2FeMoO6. Solid State Communications. 110(8):435–438. doi:10.1016/S0038-1098(99)00079-4.

Gautam P, Khare A, Sharma S, Singh NB, Mandal KD. 2016. Characterization of Bi2/3Cu3Ti4O12 ceramics synthesized by semi-wet route. Progress in Natural Science: Materials International. 26(6):567–571. doi:10.1016/j.pnsc.2016.11.008.

Gautam P, Yadava SS, Khare A, Mandal KD. 2017. Dielectric and magnetic studies of 0.5Bi2/3Cu3Ti4O12 - 0.5Bi3LaTi3O12 nano-composite ceramic synthesized by semi-wet route. Ceramics International. 43(3):3133–3139. doi:10.1016/j.ceramint.2016.11.130.

Goll D. 2007. Micromagnetism–Microstructure Relations and the Hysteresis Loop. In: Kronmüller H, Parkin S, editors. Handbook of Magnetism and Advanced Magnetic Materials. Chichester, UK: John Wiley & Sons, Ltd. p. hmm214. [accessed 2022 Jun 15]. https://onlinelibrary.wiley.com/doi/10.1002/9780470022184.hmm214.

Hamid AS, Uedono A, Chikyow T, Uwe K, Mochizuki K, Kawaminami S. 2006. Vacancy-type defects and electronic structure of perovskite-oxide SrTiO3 from positron annihilation. physica status solidi (a). 203(2):300–305. doi:10.1002/pssa.200521209.

Hao W, Zhang J, Tan Y, Su W. 2009. Giant Dielectric-Permittivity Phenomena of Compositionally and Structurally CaCu3Ti4O12-Like Oxide Ceramics. Journal of the American Ceramic Society. 92(12):2937–2943. doi:10.1111/j.1551-2916.2009.03298.x.

Hardy A, Mondelaers D, Van Bael MK, Mullens J, Van Poucke LC, Vanhoyland G, D'Haen J. 2004. Synthesis of (Bi,La)4Ti3O12 by a new aqueous solution-gel route. Journal of the European Ceramic Society. 24(6):905–909. doi:10.1016/S0955-2219(03)00420-5.

He J, Borisevich A, Kalinin SV, Pennycook SJ, Pantelides ST. 2010. Control of Octahedral Tilts and Magnetic Properties of Perovskite Oxide Heterostructures by Substrate Symmetry. Phys Rev Lett. 105(22):227203. doi:10.1103/PhysRevLett.105.227203.

Heiland G. 1954. Zum Einfluß von adsorbiertem Sauerstoff auf die elektrische Leitfähigkeit von Zinkoxydkristallen. Zeitschrift für Physik. 138(3–4):459–464.

Holtzworth-Munroe A, Jacobson NS. 1985. Causal attributions of married couples: When do they search for causes? What do they conclude when they do? Journal of Personality and Social Psychology. 48(6):1398–1412. doi:10.1037/0022-3514.48.6.1398.

Hou D, Luo W, Huang Y, Yu JC, Hu X. 2013. Synthesis of porous Bi4Ti3O12 nanofibers by electrospinning and their enhanced visible-light-driven photocatalytic properties. Nanoscale. 5(5):2028. doi:10.1039/c2nr33750a.

Huijben M, Rijnders G, Blank DHA, Bals S, Aert SV, Verbeeck J, Tendeloo GV, Brinkman A, Hilgenkamp H. 2006. Electronically coupled complementary interfaces between perovskite band insulators. Nature Mater. 5(7):556–560. doi:10.1038/nmat1675.

Huízar-Félix AM, Hernández T, de la Parra S, Ibarra J, Kharisov B. 2012. Sol–gel based Pechini method synthesis and characterization of Sm1−xCaxFeO3 perovskite 0.1≤x≤0.5. Powder Technology. 229:290–293. doi:10.1016/j.powtec.2012.06.057.

Hwang J, Rao RR, Giordano L, Katayama Y, Yu Y, Shao-Horn Y. 2017. Perovskites in catalysis and electrocatalysis. Science. 358(6364):751–756. doi:10.1126/science.aam7092.

Iliev MN, Popov VN, Litvinchuk AP, Abrashev MV, Bäckström J, Sun YY, Meng RL, Chu CW. 2005. Comparative Raman studies of , and. Physica B: Condensed Matter. 358(1–4):138–152. doi:10.1016/j.physb.2004.12.069.

Jacobson AJ, Johnson JW, Lewandowski JT. 2002 May 1. Interlayer chemistry between thick transition-metal oxide layers: synthesis and intercalation reactions of K[Ca2Nan-3NbnO3n+1] (3 .ltoreq. n .ltoreq. 7). ACS Publications. doi:10.1021/ic00217a006. [accessed 2021 Jul 12]. https://pubs.acs.org/doi/pdf/10.1021/ic00217a006.

Jang Y-I, Moorehead WD, Chiang Y-M. 2002. Synthesis of the monoclinic and orthorhombic phases of LiMnO2 in oxidizing atmosphere. Solid State Ionics. 149(3):201–207. doi:10.1016/S0167-2738(02)00176-5.

Koehler WC, Wollan EO. 1957. Neutron-diffraction study of the magnetic properties of perovskite-like compounds LaBO3. Journal of Physics and Chemistry of Solids. 2(2):100–106. doi:10.1016/0022-3697(57)90095-1.

Kong J, Yang T, Rui Z, Ji H. 2019. Perovskite-based photocatalysts for organic contaminants removal: Current status and future perspectives. Catalysis Today. 327:47–63. doi:10.1016/j.cattod.2018.06.045.

Koops CG. 1951. On the Dispersion of Resistivity and Dielectric Constant of Some Semiconductors at Audiofrequencies. Phys Rev. 83(1):121–124. doi:10.1103/PhysRev.83.121.

Kretly LC, Almeida AFL, Oliveira RS de, Sasaki JM, Sombra ASB. 2003. Electrical and optical properties of CaCu3Ti4O12 (CCTO) substrates for microwave devices and antennas. Microwave and Optical Technology Letters. 39(2):145–150. doi:10.1002/mop.11152.

Kuczenski R, Segal D. 1989. Concomitant characterization of behavioral and striatal neurotransmitter response to amphetamine using in vivo microdialysis. J Neurosci. 9(6):2051–2065.

Kumar A, Verma MK, Singh S, Das T, Singh L, Mandal KD. 2020. Electrical, Magnetic and Dielectric Properties of Cobalt-Doped Barium Hexaferrite BaFe12−xCoxO19 (x = 0.0, 0.05, 0.1 and 0.2) Ceramic Prepared via a Chemical Route. Journal of Elec Materi. 49(11):6436–6447. doi:10.1007/s11664-020-08364-8.

Kumar V, Kumar A, Verma MK, Singh S, Pandey S, Rai VS, Prajapati D, Das T, Singh NB, Mandal KD. 2020. Investigation of dielectric and electrochemical behavior of CaCu3−xMnxTi4O12 (x = 0, 1) ceramic synthesized through semi-wet route. Materials Chemistry and Physics. 245:122804. doi:10.1016/j.matchemphys.2020.122804.

Kuo D-H, Chang C-C, Su T-Y, Wang W-K, Lin B-Y. 2001. Dielectric behaviours of multi-doped BaTiO3/epoxy composites. Journal of the European Ceramic Society. 21(9):1171–1177. doi:10.1016/S0955-2219(00)00327-7.

Lachheb H, Puzenat E, Houas A, Ksibi M, Elaloui E, Guillard C, Herrmann J-M. 2002. Photocatalytic degradation of various types of dyes (Alizarin S, Crocein Orange G, Methyl Red, Congo Red, Methylene Blue) in water by UV-irradiated titania. Applied Catalysis B: Environmental. 39(1):75–90. doi:10.1016/S0926-3373(02)00078-4.

Lee HN, Visinoiu A, Senz S, Harnagea C, Pignolet A, Hesse D, Gösele U. 2000. Structural and electrical anisotropy of (001)-, (116)-, and (103)-oriented epitaxial SrBi2Ta2O9 thin films on SrTiO3 substrates grown by pulsed laser deposition. Journal of Applied Physics. 88(11):6658–6664. doi:10.1063/1.1321776.

Lemmerer A, Billing DG. 2010. Effect of heteroatoms in the inorganic–organic layered perovskite-type hybrids [(ZC $_n$ H $_{2n}$ NH $_3$) $_2$ PbI $_4$], n = 2, 3, 4, 5, 6; Z = OH, Br and I; and [(H $_3$ NC $_2$ H $_4$ S $_2$ C $_2$ H $_4$ NH $_3$)PbI $_4$]. CrystEngComm. 12(4):1290–1301. doi:10.1039/B917824D.

Lettieri J, Zurbuchen MA, Jia Y, Schlom DG, Streiffer SK, Hawley ME. 2000. Epitaxial growth of non-c-oriented SrBi2Nb2O9 on (111) SrTiO3. Appl Phys Lett. 76(20):2937–2939. doi:10.1063/1.126522.

Liu Y, Zhang M, Li L, Zhang X. 2014. One-dimensional visible-light-driven bifunctional photocatalysts based on Bi4Ti3O12 nanofiber frameworks and Bi2XO6 (X=Mo, W) nanosheets. Applied Catalysis B: Environmental. 160–161:757–766. doi:10.1016/j.apcatb.2014.06.023.

Makar JM, Tanner BK. 1998. The in situ measurement of the effect of plastic deformation on the magnetic properties of steel Part I — Hysteresis loops and magnetostriction. Journal of Magnetism and Magnetic Materials.:16.

Markovich V, Wisniewski A, Szymczak H. 2014. Chapter One - Magnetic Properties of Perovskite Manganites and Their Modifications. In: Buschow KHJ, editor. Handbook of Magnetic Materials. Vol. 22. Elsevier. p. 1–201. [accessed 2021 Jul 13]. https://www.sciencedirect.com/science/article/pii/B9780444632913000015.

Moure C, Peña O. 2015. Recent advances in perovskites: Processing and properties. Progress in Solid State Chemistry. 43(4):123–148. doi:10.1016/j.progsolidstchem.2015.09.001.

Naresh G, Mandal TK. 2014. Excellent Sun-Light-Driven Photocatalytic Activity by Aurivillius Layered Perovskites, Bi $_{5-x}$ La $_x$ Ti $_3$ FeO $_{15}$ (x = 1, 2). ACS Appl Mater Interfaces. 6(23):21000–21010. doi:10.1021/am505767c.

Pathania D, Millard M, Neamati N. 2009. Opportunities in discovery and delivery of anticancer drugs targeting mitochondria and cancer cell metabolism. Advanced Drug Delivery Reviews. 61(14):1250–1275. doi:10.1016/j.addr.2009.05.010.

Rajeswari M, Shreekala R, Goyal A, Lofland SE, Bhagat SM, Ghosh K, Sharma RP, Greene RL, Ramesh R, Venkatesan T, et al. 1998. Correlation between magnetic homogeneity, oxygen content, and electrical and magnetic properties of perovskite manganite thin films. Appl Phys Lett. 73(18):2672–2674. doi:10.1063/1.122549.

Rana S, Srivastava RS, Sorensson MM, Misra RDK. 2005. Synthesis and characterization of nanoparticles with magnetic core and photocatalytic shell: Anatase TiO2–NiFe2O4 system. Materials Science and Engineering: B. 119(2):144–151. doi:10.1016/j.mseb.2005.02.043.

Richerson DW, Lee WE. 1992. Modern Ceramic Engineering: Properties, Processing, and Use in Design, Third Edition. CRC Press.

Roy S, Dubenko IS, Khan M, Condon EM, Craig J, Ali N, Liu W, Mitchell BS. 2005. Magnetic properties of perovskite-derived air-synthesized $R\mathrm{Ba}{\mathrm{Co}}_{2}{\mathrm{O}}_{5+\ensuremath{\delta}}$ $(R=\mathrm{La}⍰\mathrm{Ho})$ compounds. Phys Rev B. 71(2):024419. doi:10.1103/PhysRevB.71.024419.

Salame P, Drai R, Prakash O, Kulkarni AR. 2014. IBLC effect leading to colossal dielectric constant in layered structured Eu2CuO4 ceramic. Ceramics International. 40(3):4491–4498. doi:10.1016/j.ceramint.2013.08.123.

Satyanarayana KG, Sukumaran K, Mukherjee PS, Pavithran C, Pillai SGK. 1990. Natural fibre-polymer composites. Cement and Concrete Composites. 12(2):117–136. doi:10.1016/0958-9465(90)90049-4.

Sharma S, M. Singh M, D. Mandal K. 2018. Microstructure, crystal structure modelling and dielectric properties of Y 2/3 Cu 3−x Zn x Ti 4 O 12 (x = 0.10, 0.20 and 0.30) ceramics. New Journal of Chemistry. 42(17):14655–14667. doi:10.1039/C8NJ02105H.

Sharma S, Yadav SS, Singh MM, Mandal KD. 2014. Impedance spectroscopic and dielectric properties of nanosized Y2/3Cu3Ti4O12 ceramic. J Adv Dielect. 04(04):1450030. doi:10.1142/S2010135X14500301.

Singh L, Rai US, Mandal KD. 2013. Dielectric properties of zinc doped nanocrystalline calcium copper titanate synthesized by different approach. Materials Research Bulletin. 48(6):2117–2122. doi:10.1016/j.materresbull.2013.02.005.

Structure–Property Relations in Rare-Earth Doped Manganite Perovskites: A Review. 2019. In: Materials Research Foundations. Vol. 57. 1st ed. Materials Research Forum LLC. p. 149–174. [accessed 2022 Jun 15]. http://www.mrforum.com/product/9781644900390-7.

Sunkara BK, Misra RDK. 2008. Enhanced antibactericidal function of W4+-doped titania-coated nickel ferrite composite nanoparticles: A biomaterial system. Acta Biomaterialia. 4(2):273–283. doi:10.1016/j.actbio.2007.07.002.

Tidrow SC. 2014. Mapping Comparison of Goldschmidt's Tolerance Factor with Perovskite Structural Conditions. Ferroelectrics. 470(1):13–27. doi:10.1080/00150193.2014.922372.

Venkatasubramanian R, Srivastava RS, Misra RDK. 2008. Comparative study of antimicrobial and photocatalytic activity in titania encapsulated composite nanoparticles with different dopants. Materials Science and Technology. 24(5):589–595. doi:10.1179/174328408X282065.

Viswanathan B. 2018. Photocatalytic Degradation of Dyes: An Overview. CCAT. 7(2):99–121. doi:10.2174/2211544707666171219161846.

Xu L, Wan Y, Xie H, Huang Y, Qiao X, Qin L, Seo HJ. 2016. On Structure, Optical Properties and Photodegradated Ability of Aurivillius-Type Bi_3TiNbO_9 Nanoparticles. Xie R-J, editor. J Am Ceram Soc. 99(12):3964–3972. doi:10.1111/jace.14423.

Yadava SS, Khare A, Gautam P, Kumar A, Mandal KD. 2017. Dielectric, ferroelectric and magnetic study of iron doped hexagonal Ba4YMn3O11.5−δ (BYMO) and its dependence on temperature as well as frequency. New J Chem. 41(11):4611–4617. doi:10.1039/C6NJ04071C.

Yadava SS, Khare A, Gautam P, Singh L, Lee Y, Mandal KD. 2016. Dielectric, ferroelectric and magnetic properties of hexagonal Ba6Y2Ti4O17 (BYTO) perovskite derived from semi wet route. RSC Adv. 6(106):104941–104948. doi:10.1039/C6RA23418F.

Yang S, Zhang H, Zhang S-W, Zhang B-P. 2011. Electrical properties tailoring in Ni-particle-dispersed (Ba0.95Ca0.05)(Ti0.96Zr0.04)O3 composites. Materials Chemistry and Physics. 126(3):729–733. doi:10.1016/j.matchemphys.2010.12.052.

Yoo C-Y, Kim J, Kim S-C, Kim S-J. 2018. Crystal structures of new layered perovskite-type oxyfluorides, CsANb2O6F (A = Sr and Ca) and comparison with pyrochlore-type CsNb2O5F. Journal of Solid State Chemistry. 267:146–152. doi:10.1016/j.jssc.2018.08.020.

Zhang L, Wang H, Chen Z, Wong PK, Liu J. 2011 May. Bi2WO6 micro/nano-structures: Synthesis, modifications and visible-light-driven photocatalytic applications. Applied Catalysis B: Environmental.:S0926337311002098. doi:10.1016/j.apcatb.2011.05.008.

Zhao M-H, Wang Z-L, Mao SX. 2004. Piezoelectric Characterization of Individual Zinc Oxide Nanobelt Probed by Piezoresponse Force Microscope. Nano Lett. 4(4):587–590. doi:10.1021/nl035198a.

Zhong W, Vanderbilt D. 1995. Competing Structural Instabilities in Cubic Perovskites. Phys Rev Lett. 74(13):2587–2590. doi:10.1103/PhysRevLett.74.2587.

Zhuk NA, Shugurov SM, Belyy VA, Makeev BA, Yermolina MV, Beznosikov DS, Koksharova LA. 2018. Thermal stability of CaCu3Ti4O12: Simultaneous thermal analysis and high-temperature mass spectrometric study. Ceramics International. 44(17):20841–20844.